The Astrophysical Journal Supplement Series, 218:6 (22pp), 2015 May doi:10.1088/0067-0049/218/1/6

THE *SPITZER* INTERACTING GALAXIES SURVEY: A MID-INFRARED ATLAS OF STAR FORMATION

N. J. Brassington[1], A. Zezas[2,3,4], M. L. N. Ashby[2], L. Lanz[2,5], Howard. A. Smith[2], S. P. Willner[2], and C. Klein[6]
[1] School of Physics, Astronomy and Mathematics, University of Hertfordshire, College Lane, Hatfield AL10 9AB, UK; n.brassington@herts.ac.uk
[2] Harvard-Smithsonian Center for Astrophysics, 60 Garden Street, Cambridge, MA 02138, USA
[3] Physics Department, University of Crete, GR-710 03 Heraklion, Crete, Greece
[4] IESL, Foundation for Research and Technology, 711 10 Heraklion, Crete, Greece
[5] Infrared Processing and Analysis Center, California Institute of Technology, MC 100-22, Pasadena, CA 91125, USA
[6] Department of Astronomy, University of California, Berkeley, CA 94720-3411, USA
Received 2014 May 29; accepted 2015 January 20; published 2015 May 6

ABSTRACT

The *Spitzer* Interacting Galaxies Survey is a sample of 103 nearby galaxies in 48 systems, selected using association likelihoods and therefore free from disturbed morphology biases. All galaxies have been observed with Infrared Array Camera and MIPS 24 μm bands from the *Spitzer Space Telescope*. This catalog presents the global flux densities and colors of all systems and correlations between the interacting systems and their specific star formation rate (sSFR). This sample contains a wide variety of galaxy interactions with systems ranging in mass, mass ratios, and gas-content as well as interaction strength. This study seeks to identify the process of triggering star formation in galaxy interactions, therefore, we focus on the non-active galactic nucleus *spiral* galaxies only. From this subset of 70 spiral galaxies we have determined that this sample has enhanced sSFR compared to a sample of non-interacting field galaxies. Through optical data we have classified each system by "interaction strength"; the strongly interacting (Stage 4) galaxies have higher sSFR values than the weakly (Stage 2) and moderately (Stage 3) interacting systems. However, the Stage 2 and 3 systems have statistically identical sSFR properties, despite the lack of optical interaction signatures exhibited by the Stage 2 galaxies. We suggest that the similarity of sSFR in these stages could be a consequence of some of these Stage 2 systems actually being post-perigalactic and having had sufficient time for their tidal features to fade to undetectable levels. This interpretation is consistent with the correlation of sSFR with separation, which we have determined to have little variation up to 100 kpc.

Key words: galaxies: evolution – galaxies: interactions – stars: formation

Supporting material: figure set

1. INTRODUCTION

Previous observational studies have suggested that there are very few galaxies that exist today that have not been influenced by an interaction with another galaxy in their past (see Struck 1999, and references therein). Many interactions trigger an increase in star formation (SF) and nuclear activity in galaxies (e.g., Larson & Tinsley 1978; Dahari 1985; Kennicutt et al. 1987; Sanders et al. 1988; Kewley et al. 2001). This behavior has also been observed in simulations (e.g., Mihos & Hernquist 1996; Di Matteo et al. 2005; Cox et al. 2006; Hopkins et al. 2008). However, not all interactions lead to this enhancement, and the strengths of these triggering mechanisms and their relation to interaction parameters are not well understood (Freedman Woods et al. 2010).

Many previous studies have been conducted to observe the evolution of galaxies undergoing interactions. Three methods are typically used to identify galaxy mergers; the first is to identify galaxies exhibiting signs of interaction through disturbed morphologies such as tidal tails and bridges. In the second, infrared (IR) luminosity cuts are made to defined thresholds to identify (ultra-) luminous IR galaxies with the implicit assumption that the luminosity is merger-induced. The third method is to select galaxy pairs based on their proximity in three dimensions.

Studies of local interacting galaxies tend to be selected on morphologies, where the tidal features of these nearby systems are readily observable (e.g Bushouse 1987; Smith et al. 2007). However, this method (as well as selecting through luminosity cuts) results in biases toward systems already undergoing obvious signs of interactions, while in contrast galaxies at the initial stages of this process do not yet exhibit tidal features nor necessarily have enhanced IR emission. Indeed, not all interactions will result in wide-scale SF, irrespective of the stage of interaction. In non-star-forming cases there will be no enhanced IR emission, and these systems will be omitted when selecting based on luminosity (cf. Kampczyk et al. 2013). The third method, often used to create larger volume samples (e.g., Woods & Geller 2007; Ellison et al. 2008; Xu et al. 2010; Huang & Hwang 2011; Scudder et al. 2012; Patton et al. 2013), avoids these biases and therefore results in a selection of both early and late stage interactions as well as those which will not give rise to significantly enhanced SF.

From recent studies based on samples of galaxy pairs, many systems involved in interactions do exhibit increased star formation rate (SFR). Xu et al. (2010) used a sample of galaxy pairs selected from cross matches between the Two Micron All Sky Survey and the Sloan Digital Sky Survey Data (SDSS) Release 3 and found enhanced specific star formation rate (sSFR; ~3 times higher sSFR than field spirals galaxies) for spiral-spiral interactions (for $M \geqslant 10^{10.5}\ M_{\odot}$). Although this sample was not selected on disturbed morphology, they only included interactions with projected separations <20 h_{75}^{-1} kpc and therefore limited the sample to systems close to the point of coalescence, which are expected to exhibit more intense star formation activity. Further, they constrained their sample to contain only major merger type events and therefore only

probed a fairly restricted area of parameter space. Scudder et al. (2012) presented a much wider array of interactions, selecting systems with separations up to 80 h_{70}^{-1} kpc (similar to the selection criteria of Ellison et al. 2008) and mass ratios of 0.1 −10. They observed an enhancement of SFR at all separations with a significant enhancement for systems <30 h_{70}^{-1} kpc. However, their selection criteria required that each galaxy has strong emission lines (to constrain metallicity), and therefore their sample did not contain galaxy pairs with no or little SF. The follow up work of Patton et al. (2013), who used a larger sample (>200,000) of galaxy pairs with separations up to 200 h_{70}^{-1} kpc, found clear evidence for increased SFR out 150 h_{70}^{-1} kpc with strong enhancement for separations <20 h_{70}^{-1} kpc, in line with previous work.

Here we use a similar proximity-based selection to create a sample of nearby interacting systems which we can study in detail, free from disturbed morphological bias. The sample includes galaxies not yet undergoing tidal influences from their companion up to strongly interacting systems. Our focus in this work is to identify the level and distribution of SF triggered in these interactions. Many previous studies of SF in local interacting galaxies have used visible observations, which in these dust-enshrouded systems are often affected by extinction (Dopita et al. 2002). Studies have also been conducted using IR imaging, initially with the *Infrared Astronomical Satellite* (*IRAS*; e.g., Kennicutt et al. 1987; Lutz 1992). *IRAS*, with its limited spatial resolution, provided global values of SFR, in many cases where the individual galaxies were not well separated these were only a single value. In the last decade, with the advent of both the *Spitzer Space Telescope* (*SST*) and the *Herschel Space Observatory*, the distribution of SF in some interacting galaxies has been studied in much greater detail (e.g., Calzetti et al. 2005; Li et al. 2013).

The level and distribution of SF in local interactions selected through association likelihoods has not been systematically studied in the IR before. We have therefore studied a sample that will allow us to identify the initial increase in SFR caused by the interaction. We can also identify where this enhancement is located in the galaxies (i.e., in the central region of the galaxy, along the disc, or within tidal features), although the SFR spatial distribution is not the focus in this article. Such a detailed study is possible only for local galaxies, where there is sufficient resolution to identify these spatial variations. Further, such a sample provides a natural complement to other local IR studies based on morphological disturbances (e.g., Smith et al. 2007).

In this study we have used mid-infrared (MIR) data, obtained with *Spitzer*, which, with its greater spatial resolution allows us to probe the galaxies in detail. In addition to this catalog paper, the properties of a subset of this sample (31 galaxies in 14 systems) derived from multi-wavelength spectral energy distribution (SED) fitting of the broadband photometry (including *Herschel* through to *GALEX* or *Swift* data), have already been presented (Lanz et al. 2013) and compared to hydrodynamic simulations (Lanz et al. 2014).

This paper provides an overview of our sample, the *Spitzer* Interacting Galaxies Survey (SIGS), and present the global Infrared Array Camera (IRAC) and MIPS 24 μm photometry for all 48 systems, comprising 103 galaxies. It is organized as follows: Section 2 discusses our sample selection and provides basic properties of all galaxies. Section 3 details the data analysis and Section 4 provides the MIR properties of our sample. Section 5 presents the sSFR for each galaxy and investigates correlations with each system and its interaction properties. A discussion of the properties of the sample are presented in Section 6, and our conclusions are given in Section 7.

2. SAMPLE SELECTION AND CHARACTERIZATION

To gain an understanding of the parameters that influence the level of activity triggered during galaxy interactions it is essential to include not only systems with obvious signs of disturbance but also galaxies that are likely to be gravitationally influencing each other but are not clearly tidally disturbed. To address this, the sample in this work is based upon association likelihoods, thus ensuring that both early-stage interactions of, potentially, major mergers, as well as interactions resulting in low-level SFR enhancement are included.

SIGS has been selected from the (Keel et al. 1985, hereafter K85) list, which identified a sample of "*interacting spiral galaxies*," termed the "Complete" sample, and a sample of more strongly interacting galaxies, referred to as the "Arp" sample. The "Complete" sample was selected to contain a spiral galaxy with a *probable* interacting companion(s), independently of the appearance of the galaxies. This selection was made from the Uppsala Galaxy Catalog based on the local galaxy density, projected separation (typically 4–5 effective radii), and relative velocity ($\delta V < 600\,\mathrm{km\ s^{-1}}$) with a magnitude limit of $B_T \leqslant 13.0$ also imposed. The "Arp" sample was selected to include additional systems exhibiting more obvious signs of interaction to probe the effects of stronger encounters. Systems with evidence of tidal distortions were selected from the *Atlas of Peculiar Galaxies* (Arp 1966), although to avoid biases toward later stage mergers, only systems still exhibiting spiral morphologies (i.e., disks that are still mostly intact) were included. From these two samples we have further imposed a limit of $cz < 4000\,\mathrm{km\ s^{-1}}$ to allow us to resolve structures of a few hundred pc with *Spitzer* IRAC. Additionally, we have included fainter companions within interacting systems that were excluded in the K85 sample. This provides a more complete census of how interactions influence the star-forming properties over a large range of galaxy masses. The final sample contains 103 individual galaxies in 48 interacting systems. Sixty-five of these galaxies belong to the Complete sample with the Arp sample comprising the remaining 38 systems. Our sample containing both these subsamples provides us with a built-in comparison on the effects of SF between weakly and strongly interacting galaxies.

The list of galaxies is presented in Table 1, alongside their basic properties. As all of our galaxies are within $cz < 4000\,\mathrm{km\ s^{-1}}$ and are likely to be involved in interactions, the peculiar velocities of some of these systems are comparable with their Hubble flow velocities. We have therefore sought to use redshift-independent distance measurements where possible. These values were primarily taken from Tully et al. (2008), who used a combination of alternative methods (e.g., Tully–Fisher relation, Cepheids, tip of the red giant branch, surface brightness fluctuations) to determine distance measurements for galaxies within $V < 3000\,\mathrm{km\ s^{-1}}$. Additional galaxy distances were based on their group or cluster associations, which are given in the Extra-galactic Distance Database[7] (EDD; R. B. Tully 2010, private communication). For the

[7] http://edd.ifa.hawaii.edu

Table 1
Basic Properties of All SIGS Galaxies

GrpID	Galaxy	Arp Name	R.A. (J2000.0)	Decl. (J2000.0)	Distance (Mpc)	Sample	Interaction Strength	Morphological Classification	Nuclear Activity	Separation (kpc)
(1)	(2)	(3)	(4)	(5)	(6)	(7)	(8)	(9)	(10)	(11)
Grp1	NGC 274	140	00:51:01.87	−07:03:25.39	19.50	A	4.0 ± 0.5	S0	⋯	4.46
Grp1	NGC 275	140	00:51:04.29	−07:03:56.02	21.88	A	4.0 ± 0.5	Scd	H	4.46
Grp2	NGC 470	227	01:19:44.84	03:24:34.86	36.14	A	2.0 ± 0.5	Sb	H	57.34
Grp2	NGC 474	227	01:20:06.65	03:24:56.02	32.51	A	2.0 ± 0.5	S0	L	57.34
Grp3	NGC 520	157	01:24:34.62	03:47:31.76	27.80	A	5.0 ± 0.5	Pec(E+S)	H	5.39
Grp4	IC 195	290	02:03:44.6	14:42:33	49.03 [a]	A	3.0 ± 0.5	S0	H	31.12
Grp4	IC 196	290	02:03:49.8	14:44:21	49.00 [a]	A	3.0 ± 0.5	SBb	L	31.12
Grp5	NGC 833	318/HCG 16	02:09:20.9	−10:08:00	51.96 [a]	A	4.0 ± 0.5	Sa	L	14.35
Grp5	NGC 835	318/HCG 16	02:09:24.7	−10:08:11	54.79 [a]	A	4.0 ± 0.5	Sab	L/H	14.35
Grp5	NGC 838	318/HCG 16	02:09:38.5	−10:08:49	51.79 [a]	A	3.0 ± 0.5	Sa	H	37.01
Grp5	NGC 839	318/HCG 16	02:09:42.9	−10:11:03	52.09 [a]	A	2.0 ± 0.5	Im	H/L	37.01
Grp6	IC 1801	276	02:28:12.79	19:34:59.27	54.12 [a]	A	4.0 ± 0.5	SBb	H	16.20
Grp6	NGC 935	276	02:28:11.17	19:35:56.54	55.72 [a]	A	4.0 ± 0.5	Scd	L	16.20
Grp7	NGC 1241	304	03:11:14.6	−08:55:20	53.00 [a]	A	3.0 ± 0.5	SBb	L	25.54
Grp7	NGC 1242	304	03:11:19.3	−08:54:09	52.99 [a]	A	3.0 ± 0.5	SBc	H	25.54
Grp8	NGC 1253	279	03:14:09.0	−02:49:23	20.89	A	3.0 ± 0.5	Scd	H	23.42
Grp8	NGC 1253 A	279	03:14:23.3	−02:48:03	24.57 [a]	A[b]	3.0 ± 0.5	Sm	⋯	23.42
Grp9	NGC 2276	025	07:27:14.3	85:45:20.02	36.81	C	2.0 ± 0.5	Sc	H	⋯
Grp10	NGC 2444	143	07:46:53.04	39:01:54.52	58.99 [a]	A	4.0 ± 0.5	E	⋯	20.36
Grp10	NGC 2445	143	07:46:54.94	39:00:46.73	58.36 [a]	A	4.0 ± 0.5	Sring	H	20.36
Grp11	NGC 2633	080	08:48:04.6	74:05:56	33.27	C	2.0 ± 0.4	SBb	H	78.07
Grp11	NGC 2634	080	08:48:25.4	73:58:01	32.62	C[b]	2.0 ± 0.5	E	⋯	17.93
Grp11	NGC 2634 A	080	08:48:38.1	73:56:21	34.25	C[b]	2.0 ± 0.5	Sbc	⋯	17.93
Grp12	NGC 2719	202	09:00:15.4	35:43:40	49.98	A	2.0 ± 0.5	Im	H	6.45
Grp12	NGC 2719 A	202	09:00:15.9	35:43:12	48.39	A	2.0 ± 0.5	Im	H	6.45
Grp13	NGC 2805	⋯	09:20:20.16	64:06:02.05	28.05	C	2.0 ± 0.5	Sd	H	85.63
Grp13	NGC 2814	⋯	09:21:11.5	64:15:4.9	27.16	C	2.0 ± 0.5	Sb	H	85.63
Grp14	NGC 2820	⋯	09:21:45.77	64:15:28.33	26.06	C	3.0 ± 0.5	SBc	⋯	15.81
Grp14	NGC 2820 A	⋯	09:21:30.3	64:14:20.0	24.66	C[b]	3.0 ± 0.5	I0	⋯	15.81
Grp15	NGC 2964	⋯	09:42:54.26	31:50:50.82	21.88	C	2.0 ± 0.5	Sbc	H	39.30
Grp15	NGC 2968	⋯	09:43:12.07	31:55:42.96	25.82	C	2.0 ± 0.5	I0	⋯	39.30
Grp15	NGC 2970	⋯	09:43:31.06	31:58:37.42	26.67	C	2.0 ± 0.5	E	⋯	36.01
Grp16	NGC 2976	⋯	09:47:14.59	67:55:01.42	3.75	C	2.0 ± 0.0	Sc	H[c]	⋯
Grp17	NGC 3031	M81	09:55:33.22	69:03:42.66	3.77	C	2.0 ± 0.4	Sab	L/S	40.42
Grp17	NGC 3034	337/M82	09:55:51.84	69:40:49.0	3.89	C[b]	2.0 ± 0.4	Im	H[c]	40.42
Grp17	NGC 3077	⋯	10:03:19.94	68:44:01.36	3.93	C	2.0 ± 0.5	Im	H	50.96
Grp18	NGC 3165	⋯	10:13:31.27	03:22:31.75	24.86	C[b]	3.0 ± 0.5	Sdm	⋯	33.50
Grp18	NGC 3166	⋯	10:13:45.79	03:25:29.73	21.98	C	3.0 ± 0.5	Sa	L	49.55
Grp18	NGC 3169	⋯	10:14:15.05	03:27:57.79	19.68	C	2.0 ± 0.5	Sa	L	49.55
Grp19	NGC 3185	HCG 44	10:17:38.49	21:41:14.74	22.59	C	2.0 ± 0.5	SBa	S	74.13
Grp19	NGC 3187	316/HCG 44	10:17:47.88	21:52:22.26	26.06	C[b]	3.0 ± 0.5	SBc	⋯	74.13
Grp19	NGC 3190	316/HCG 44	10:18:05.66	21:49:56.64	22.49	C	3.0 ± 0.5	Sa	L	70.29
Grp20	NGC 3226	094	10:23:27.05	19:53:53.66	23.55	C	4.0 ± 0.5	E	L	14.56
Grp20	NGC 3227	094	10:23:30.53	19:51:54.97	20.61	C	4.0 ± 0.5	SBa	S	14.56
Grp21	NGC 3395	270	10:49:50.1	32:58:58	27.73	C	4.0 ± 0.5	SBcd	H	9.75
Grp21	NGC 3396	270	10:49:55.9	32:59:27	27.73	C	4.0 ± 0.5	Im	H	9.75
Grp22	NGC 3424	⋯	10:51:46.3	32:54:03.0	26.06	C	2.0 ± 0.4	SBb	H	46.02
Grp22	NGC 3430	⋯	10:52:11.4	32:57:02.0	26.67	C	2.0 ± 0.4	SBc	H	46.02
Grp23	NGC 3448	205	10:54:39.2	54:18:19	24.43	A[b]	3.0 ± 0.0	Im	H[c]	27.49
Grp23	UGC 6016	205	10:54:13.5	54:17:14	27.07 [a]	A[b]	3.0 ± 0.0	Im	⋯	27.49
Grp24	IC 694	299	11:28:27.31	58:34:42.13	48.07 [a]	C	4.0 ± 0.5	Sc	H	4.93
Grp24	NGC 3690	299	11:28:33.65	58:33:45.65	48.07 [a]	C	4.0 ± 0.4	Sc	H	4.93
Grp25	NGC 3786	294	11:39:42.5	31:54:33	41.69	C	3.0 ± 0.5	Sa	S	17.02
Grp25	NGC 3788	294	11:39:44.6	31:55:52	36.48	C	3.0 ± 0.5	Sab	⋯	17.02
Grp26	NGC 3799	083	11:40:09.43	15:19:38.53	53.02 [a]	A	3.0 ± 0.4	SBb	H	20.66
Grp26	NGC 3800	083	11:40:13.46	15:20:32.42	53.02 [a]	A	3.0 ± 0.4	Sb	H/L	20.66
Grp27	IC 749	⋯	11:58:33.96	42:44:02.65	16.98	C	2.0 ± 0.5	SBcd	H	16.84
Grp27	IC 750	⋯	11:58:52.18	42:43:19.92	23.29	C	2.0 ± 0.5	Sab	H	16.84
Grp28	NGC 4038/4039	244(Anten)	12:01:55.03	−18:52:33.71	25.41	A	4.0 ± 0.0	SBm/Sm	H/H	9.31
Grp29	NGC 4382	M85	12:25:23.95	18:11:27.06	17.86	C[b]	2.0 ± 0.4	S0	⋯	39.50
Grp29	NGC 4394	⋯	12:25:55.61	18:12:50.72	16.83	C	2.0 ± 0.4	SBb	L	39.50

Table 1
(Continued)

GrpID	Galaxy	Arp Name	R.A. (J2000.0)	Decl. (J2000.0)	Distance (Mpc)	Sample	Interaction Strength	Morphological Classification	Nuclear Activity	Separation (kpc)
(1)	(2)	(3)	(4)	(5)	(6)	(7)	(8)	(9)	(10)	(11)
Grp30	NGC 4567	⋯	12:36:32.7	11:15:28	16.83	C	3.0 ± 0.5	Sbc	H/L	5.67
Grp30	NGC 4568	⋯	12:36:34.3	11:14:19	16.83	C	3.0 ± 0.5	Sbc	H	5.67
Grp31	NGC 4618	023	12:41:32.83	41:08:44.23	6.70	C	3.0 ± 0.5	SBm	H	16.43
Grp31	NGC 4625	023	12:41:52.37	41:16:20.93	8.20	C	3.0 ± 0.5	SBm	H	16.43
Grp32	NGC 4647	116	12:43:32.78	11:34:52.93	16.83	C	3.0 ± 0.5	SBc	H	12.04
Grp32	NGC 4649	116/M60	12:43:39.96	11:33:09.54	17.30	C[b]	3.0 ± 0.5	E	⋯	12.04
Grp33	NGC 4933 A	176	13:03:54.58	−11:30:20.02	47.84	A	4.0 ± 0.4	E	L	11.23
Grp33	NGC 4933 B	176	13:03:57.02	−11:29:48.19	49.84	A	4.0 ± 0.4	S0	⋯	11.23
Grp33	NGC 4933 C	176	13:04:01.08	−11:29:26.22	48.08	A[b]	4.0 ± 0.6	Im	⋯	25.33
Grp34	NGC 5194	85/M51A	13:29:53.42	47:11:46.25	7.69	C	3.0 ± 0.5	Sbc	L	9.60
Grp34	NGC 5195	85/M51B	13:29:59.66	47:15:58.5	7.66	C	3.0 ± 0.5	Im	H	9.60
Grp35	NGC 5350	HCG 68	13:53:21.72	40:21:51.87	37.84	C	3.0 ± 0.5	SBb	L	54.10
Grp35	NGC 5353	HCG 68	13:53:26.69	40:16:59.48	37.84	C	3.0 ± 0.5	S0	L	14.35
Grp35	NGC 5354	HCG 68	13:53:26.71	40:18:09.5	42.07 [a]	C[b]	2.0 ± 0.5	S0	L/T‡	14.35
Grp36	NGC 5394	84	13:58:33.6	37:27:13	56.38 [a]	C	4.0 ± 0.5	SBb	H	29.72
Grp36	NGC 5395	84	13:58:37.9	37:25:28	56.38 [a]	C	4.0 ± 0.5	Sb	L	29.72
Grp37	NGC 5457	026/M101	14:03:09.98	54:20:38.65	6.70	C	3.0 ± 0.6	SBcd	H	86.83
Grp37	NGC 5474	⋯	14:05:01.22	53:39:11.45	5.94	C	3.0 ± 0.6	Scd	H	86.83
Grp38	NGC 5426	271	14:03:24.8	−06:04:09	35.81	A	4.0 ± 0.5	Sc	H	24.59
Grp38	NGC 5427	271	14:03:26.0	−06:01:51	38.19	A	4.0 ± 0.5	Sc	S	24.59
Grp39	NGC 5480	⋯	14:06:21.55	50:43:26.54	31.92	C	2.0 ± 0.5	Sc	H	29.13
Grp39	NGC 5481	⋯	14:06:41.2	50:43:24	35.65	C	2.0 ± 0.5	E	⋯	29.13
Grp40	NGC 5544	199	14:17:02.66	36:34:17.69	51.44 [a]	C	3.0 ± 0.5	S0	L	8.51
Grp40	NGC 5545	199	14:17:05.18	36:34:30.72	52.00 [a]	C	3.0 ± 0.5	Sbc	L	8.51
Grp41	NGC 5614	178	14:24:07.56	34:51:32.58	62.27 [a]	C	4.0 ± 0.5	Sab	L	7.61
Grp41	NGC 5615	178	14:24:06.5	34:51:53.68	62.98 [a]	C	4.0 ± 0.5	Compact	H	7.61
Grp42	NGC 5846	⋯	15:06:29.28	01:36:20.28	24.89	C[b]	2.0 ± 0.5	E	T[c]	72.99
Grp42	NGC5846A	⋯	15:06:29.20	01:35:42:00	24.89	C[b]	2.0 ± 0.5	E	⋯	4.65
Grp42	NGC 5850	⋯	15:07:07.75	01:32:41.37	28.44	C	2.0 ± 0.5	SBb	L	72.99
Grp43	NGC 5905	⋯	15:15:23.23	55:31:01.96	53.98 [a]	C	3.0 ± 0.5	SBb	H	205.21
Grp43	NGC 5908	⋯	15:16:43.25	55:24:33.12	52.83 [a]	C	2.0 ± 0.5	Sb	L	205.21
Grp44	NGC 5929	090	15:26:06.1	41:40:14	38.55	C	4.0 ± 0.5	Sab	S	5.18
Grp44	NGC 5930	090	15:26:07.9	41:40:34	41.88	C	4.0 ± 0.5	SBb	H	5.18
Grp45	NGC 5953	091	15:34:32.38	15:11:37.79	32.96	A	4.0 ± 0.5	Sa	S	7.15
Grp45	NGC 5954	091	15:34:34.94	15:12:01.69	32.06	A	4.0 ± 0.5	SBcd	H	7.15
Grp46	NGC 5981	⋯	15:37:52.7	59:23:38	29.24	C	2.0 ± 0.4	Sc	⋯	116.41
Grp46	NGC 5985	⋯	15:39:37.1	59:19:55	39.26	C	2.0 ± 0.4	SBb	L	116.41
Grp47	Arp 314 A	⋯	22:58:02.14	−03:46:11.13	51.70 [a]	A	4.0 ± 0.4	S	H	26.88
Grp47	Arp 314 B	⋯	22:58:07.61	−03:47:19.38	51.70 [a]	A	4.0 ± 0.4	S	H	26.88
Grp47	Arp 314 C	⋯	22:58:07.34	−03:48:38.11	51.70 [a]	A[b]	4.0 ± 0.4	Im	⋯	19.75
Grp48	NGC 7714	284	23:36:14.21	02:09:17.61	36.81	A	4.0 ± 0.5	SBb	H	19.15
Grp48	NGC 7715	284	23:36:21.73	02:09:23.11	36.31	A	4.0 ± 0.5	Im	H	19.15

Note. Columns 1, 2, and 3, provide our group numbering scheme (group refers to each of the interacting systems, ranging from individual galaxies up to systems containing four individual galaxy members. This term does not refer to defined cosmological groups.), each galaxy's NGC identifier (or alternative naming) and the galaxy's Arp name (or other if available) respectively. Columns 4 and 5 provide the R.A. and Decl. Column 6 presents distances; those determined from heliocentric velocities are indicated by a, assuming $H_0 = 72$ km s^{-1} Mpc^{-1}. Information in column (7) indicates the sub-sample from which each galaxy is drawn; C indicates the Complete sample and A the Arp sample. A b indicates that the galaxy was not included in the original sample. The interaction strength is a median value and standard deviation of the characterization from 6 independent classifications and is discussed in Section 2. Galaxy morphology classifications are taken from RC3 (de Vaucouleurs et al. 1991). Column (10) presents the nuclear spectral activity classified based on optical spectra, taken from K85 (or Ho et al. 1997 when indicated by a c.) H indicates an H II or star-forming nuclei, L a Low Ionization Narrow Emission Line Region (LINER), S a Seyfert galaxy, and T a transition object that has been assumed to be a LINER/H II. Column (11) provides the projected separation in kpc between the galaxies in each group. For instances where there are more than two galaxies within one system, separations quoted are primarily between the more massive galaxies, with separation for the less massive galaxies taken to be the nearest massive galaxy (e.g., Grp42).

remaining galaxies we obtained heliocentric velocities from the PSCz (Saunders et al. 2000) or RC3 catalogs (de Vaucouleurs et al. 1991), which were corrected to account for the velocity field of Virgo, the Great Attractor and the Shapley supercluster following Mould et al. (2000). Distances were then calculated assuming $H_0 = 72$ km s^{-1} Mpc^{-1}.

To probe the influence of interactions on sSFR we have classified the "interaction strength" of each galaxy based on its visible appearance. The classification scheme divides the interactions into five stages and is based upon the scheme presented by Dopita et al. (2002). In their scheme Stage 1 galaxies are isolated systems and therefore not in our sample.

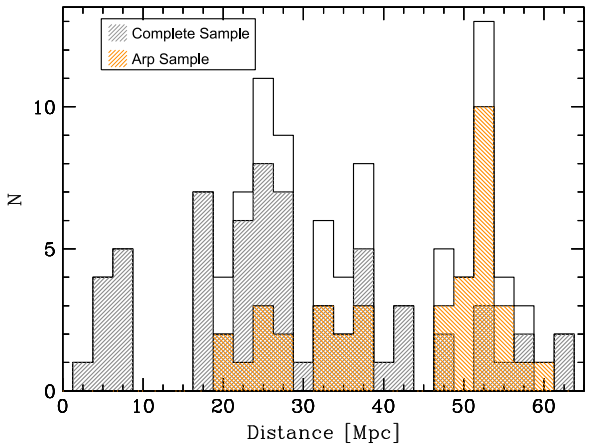

Figure 1. Histogram of the distance distribution of all 103 galaxies in the sample is indicated by the open histogram. The distance distribution of the "Complete" and "Arp" samples are represented by the gray and orange histograms, respectively.

The Stage 2 systems are weakly interacting, probably gravitationally bound, but exhibiting low or no morphological distortions. Stage 3 systems are moderately interacting and have mild morphological distortions with some tidal features. Stage 4 systems are strongly interacting with prominent tidal features but still present separate nuclei, and Stage 5 systems are mergers at the point of coalescence or merger remnants, where separate nuclei cannot be identified on the Digitized Sky Survey (DSS) images alone. These classifications were carried out independently by six collaborators using the DSS images. The median values and standard deviations for each galaxy are provided in Table 1. For systems with more than two galaxies, classifications were defined for each group member.

In Table 1 there are two groups (Grp9 and Grp16) that contain only a single member. These galaxies were included in the K85 paper as both are found within a group environment but are sufficiently distant from other group members that their gravitational influence will not significantly influence the other systems' evolution: NGC 2276 (Grp9), lies within the NGC 2300 group, and NGC 2976 (Grp16), is part of the M81 group. However, the influence of the group is enough to affect the activity of the system. In instances where there are more than two members in a group separations quoted are primarily between the more massive galaxies with separation for the less massive galaxies taken to be the nearest massive galaxy, which will have the strongest tidal effect on the less massive companions (e.g., Grp42).

The distance distribution of all 103 galaxies is presented in Figure 1. The systems in our sample range from just over 3 Mpc out to ~63 Mpc, the Arp galaxies tend to reside at slightly larger distances than those in the Complete sample.

3. DATA REDUCTION AND ANALYSIS

All 103 galaxies in the SIGS sample were observed with the IRAC (Fazio et al. 2004) and the Multiband Imaging Photometer (MIPS; Rieke et al. 2004) on the *SST*. These observations were obtained through both the archive and our observing program (PID 20140; PI A. Zezas). A log of all observations is presented in Table 2.

The basic calibrated data (BCD) used for post-pipeline processing were obtained from the archive with pipeline versions ranging from S13 to S18. To investigate the consistency in the final data products between the pipeline versions we have compared photometry from some systems obtained with the S13 pipeline to the same data processed with the S18 pipeline. All photometry differs by <2% (i.e., less than the standard IRAC calibration uncertainty). A small correction has been applied to the 5.8 μm and 8.0 μm data obtained from the S18.18.0 pipeline to correct photometric calibration errors caused by the use of incorrect color corrections for the calibration stars.[8]

3.1. IRAC Images

IRAC observations were obtained with all four of the broadband filters: 3.6, 4.5, 5.8, and 8.0 μm. For all systems we carried out analysis on the *Spitzer* Science Center's (SSCs) pipeline produced BCD images. The data were processed using the IRACproc package (Schuster et al. 2006), which augments the SSC's mosaicing software MOPEX, providing a more effective outlier rejection technique. All mosaics were produced with a resolution of 0.″6. These initial mosaics were inspected for image artifacts such as banding, muxbleed, striping, and column pulldown, and the corresponding BCD images were corrected using the software package *imclean*.[9] From these cleaned frames the final mosaics were produced, using all frame times available in the AORs (Astronomical Observing Request). For some systems with bright nuclear emission the longer exposure frames were saturated in the nucleus, and mosaics were created using the shorter exposures from the high dynamic range (HDR) mode data where available (see Section 3.3 for saturation correction details).

From these mosaics, in addition to the four IRAC passbands, a non-stellar (NS) 8.0 μm image was also produced. The 8.0 μm band image is dominated by polycyclic aromatic hydrocarbons (PAHs) but also has a small contribution from stellar continuum. To remove this stellar emission a scaled 3.6 μm image (where the emission is generated by stellar photospheres) was subtracted from the 8.0 μm image. A scaling factor of 0.26 was used (Wu et al. 2005). Figure 2 shows composite images for seven interacting systems in our sample. Figure 3 shows images from three separate filters for all 103 galaxies.[10]

Global photometry was carried out for all 103 SIGS galaxies with SExtractor (version 2.8.6; Bertin & Arnouts 1996). Across the four IRAC bands the morphology of the galaxies can be significantly different, and we therefore used SExtractor to determine apertures for each band on all galaxies. These were then compared to identify which band exhibited the most extended emission. In all cases this was the 3.6 μm band, which we subsequently used for consistency to perform source detection and characterization for each galaxy using the SExtractor two-image mode. Photometry was carried out on all four IRAC bands as well as the NS image. The background was estimated automatically by SExtractor, where the

[8] For full details see memo http://irsa.ipac.caltech.edu/data/SPITZER/docs/irac/s18.18fluxconv.shtml

[9] This software has been developed by Joseph L. Hora and can be obtained from http://irsa.ipac.caltech.edu/data/SPITZER/docs/dataanalysistools/tools/contributed/irac/imclean/

[10] For Grp24, in addition to the two galaxies that are defined to comprise Arp 299 (IC 694 and NGC 3690), the dwarf irregular MCG+10172a is also labelled for clarity, as historically there has been confusion about which of these three systems are IC 694 and NGC 3690. Due to the saturation problems with this group the dwarf system is not included in the present study and therefore does not feature further in this work.

Table 2
Spitzer Observations Log

GrpID	Galaxy	IRAC PID	Date	Exposure	Pipeline	MIPS PID	Date	Mode	Exposure	Pipeline
(1)	(2)	(3)	(4)	(5)	(6)	(7)	(8)	(9)	(10)	(11)
Grp1	NGC 274	20140	2005 Dec	10 × 30	14.0.0	50696	2008 Aug	Phot	660.2	18.1.0
Grp1	NGC 275	20140	2005 Dec	10 × 30	14.0.0	50696	2008 Aug	Phot	660.2	18.1.0
Grp2	NGC 470	20140	2005 Dec	20 × 30	14.0.0	20140	2006 Jan	Phot	1184.2	14.4.0
Grp2	NGC 474	20140	2005 Dec	20 × 30	14.0.0	20140	2006 Jan	Phot	1184.2	14.4.0
Grp3	NGC 520	32	2003 Dec	60 × 12	13.2.0	32	2005 Jan	Phot	330.1	14.4.0
Grp4	IC 195	30406	2006 Aug	32 × 30	18.12.0	3247	2005 Jan	Phot	312.5	14.4.0
Grp4	IC 195	3247	2005 Jan	72 × 12	18.12.0	…	…	…	…	…
Grp4	IC 196	30406	2006 Aug	32 × 30	18.12.0	3247	2005 Jan	Phot	312.5	14.4.0
Grp4	IC 196	3247	2005 Jan	72 × 12	18.12.0	…	…	…	…	…
Grp5	NGC 833	3596,3672	2005 Jan	88 × 30	18.7.0	3596	2004 Dec	Phot	1587.7	14.4.0
Grp5	NGC 835	3596,3672	2005 Jan	88 × 30	18.7.0	3596	2004 Dec	Phot	1587.7	14.4.0
Grp5	NGC 838	3596,3672	2005 Jan	88 × 30	18.7.0	3596	2004 Dec	Phot	1587.7	14.4.0
Grp5	NGC 839	3596,3672	2005 Jan	88 × 30	18.7.0	3596	2004 Dec	Phot	1587.7	14.4.0
Grp6	IC 1801	20140	2006 Feb	10 × 30	14.0.0	20140	2006 Feb	Phot	691.7	14.4.0
Grp6	NGC 935	20140	2006 Feb	10 × 30	14.0.0	20140	2006 Feb	Phot	691.7	14.4.0
Grp7	NGC 1241	3269	2005 Jan	2 × 12	18.18.0	20140	2006 Feb	Phot	896.0	14.4.0
Grp7	NGC 1242	3269	2005 Jan	2 × 12	18.18.0	20140	2006 Feb	Phot	896.0	14.4.0
Grp8	NGC 1253	3247	2005 Jan	72 × 12	18.7.0	3247	2005 Jan	Phot	312.5	14.4.0
Grp8	NGC 1253A	3247	2005 Jan	72 × 12	18.7.0	3247	2005 Jan	Phot	312.5	14.4.0
Grp9	NGC 2276	20140	2005 Dec	20 × 30	14.0.0	20140	2005 Nov	Phot	712.6	14.4.0
Grp10	NGC 2444	218	2005 Mar	48 × 12	13.2.0	40410	2007 Nov	Phot	110.0	14.4.0
Grp10	NGC 2445	218	2005 Mar	48 × 12	13.2.0	40410	2007 Nov	Phot	110.0	14.4.0
Grp11	NGC 2633	20140	2006 Oct	20 × 12	18.7.0	20140	2005 Nov	Phot	1079.4	14.4.0
Grp11	NGC 2634	20140	2006 Oct	20 × 12	18.7.0	20140	2005 Nov	Phot	1079.4	14.4.0
Grp11	NGC 2634A	20140	2006 ct	20 × 12	18.7.0	20140	2005 Nov	Phot	1079.4	14.4.0
Grp12	NGC 2719	3247	2005 May	47 × 12	18.18.0	3247	2004 Nov	Phot	312.5	14.4.0
Grp12	NGC 2719A	3247	2005 May	47 × 12	18.18.0	3247	2004 Nov	Phot	312.5	14.4.0
Grp13	NGC 2805	20140	2005 Nov	32 × 30	14.0.0	20140	2005 Nov	Phot	1063.7	14.4.0
Grp13	NGC 2814	20140	2005 Nov	32 × 30	14.0.0	20140	2005 Nov	Phot	1063.7	14.4.0
Grp14	NGC 2820	20140	2005 Nov	32 × 30	14.0.0	250696	2008 Apr	Phot	880.3	17.2.0
Grp14	NGC 2820A	20140	2005 Nov	32 × 30	14.0.0	250696	2008 Apr	Phot	880.3	17.2.0
Grp15	NGC 2964	69,20140	2004 Dec,2005 Nov	30 × 30	14.0.0	20140	2005 Dec	Phot	1771.1	14.4.0
Grp15	NGC 2968	69,20140	2004 Dec,2005 Nov	30 × 30	14.0.0	20140	2005 Dec	Phot	1771.1	14.4.0
Grp15	NGC 2970	69,20140	2004 Dec,2005 Nov	30 × 30	14.0.0	20140	2005 Dec	Phot	1771.1	14.4.0
Grp16	NGC 2976	159	2004 Oct	30 × 30	13.2.0	159	2004 Oct	Scan	169.8	14.4.0
Grp17	NGC 3031	159	2004 May	240 × 30	13.0.2	159	2003 Nov	Scan	175.8	14.4.0
Grp17	NGC 3034	159	2005 May	120 × 30	14.0.0	159	2004 Nov	Scan	152.5	14.4.0
Grp17	NGC 3077	59	2004 Mar	8 × 12	18.18.0	59	2004 Mar	Phot	159.3	18.13.0
Grp17	NGC 3077	40204	2007 Nov	22 × 30	18.18.0	…	…	…	…	…
Grp18	NGC 3165	3674,20140	2004 Nov,2005 Dec	26 × 30	14.0.0	20140	2005 Dec	Phot	848.9	14.4.0
Grp18	NGC 3166	3674,20140	2004 Nov,2005 Dec	26 × 30	14.0.0	20140	2005 Dec	Phot	848.9	14.4.0
Grp18	NGC 3169	3674,20140	2004 Nov,2005 Dec	26 × 30	14.0.0	20140	2005 Dec	Phot	848.9	14.4.0
Grp19	NGC 3185	40936	2007 Dec	8 × 12	18.18.0	159	2004 Dec	Scan	173.3	14.4.0
Grp19	NGC 3187	159	2004 Apr	48 × 30	13.2.0	159	2004 Dec	Scan	156.2	14.4.0
Grp19	NGC 3190	159	2004 Apr	48 × 30	13.2.0	159	2004 Dec	Scan	176.6	14.4.0
Grp20	NGC 3226	1054,3269	2003 Nov,2004 Dec	50 × 12	13.2.0	1054	2003 Nov	Phot	593.4	14.4.0
Grp20	NGC 3227	1054,3269	2003 Nov,2004 Dec	50 × 12	13.2.0	1054	2003 Nov	Phot	593.4	14.4.0
Grp21	NGC 3395	20671	2006 Dec	24 × 12	18.7.0	20140	2005 Dec	Phot	226.4	14.4.0
Grp21	NGC 3396	20671	2006 Dec	24 × 12	18.7.0	20140	2005 Dec	Phot	226.4	14.4.0
Grp22	NGC 3424	20140	2006 Jun	30 × 12	14.0.0	50696	2008 Jun	Phot	220.1	18.13.0
Grp22	NGC 3430	20140	2006 Jun	30 × 12	14.0.0	50696	2008 Jun	Phot	542.3	18.13.0
Grp23	NGC 3448	3247	2004 Dec	72 × 12	14.0.0	3247	2007 Jun	Phot	557.8	14.4.0
Grp23	UGC6016	3247	2004 Dec	72 × 12	14.0.0	3247	2007 Jun	Phot	557.8	14.4.0
Grp24	IC694	32,108	2003 Dec,2004 May-2005 May	192 × 12	13.2.0	32	2005 Jan	Phot	79.6	14.4.0
Grp24	NGC 3690	32,108	2003 Dec,2004 May-2005 May	192 × 12	13.2.0	32	2005 Jan	Phot	79.6	14.4.0
Grp25	NGC 3786	3247	2004 Dec	46 × 12	14.0.0	3247	2005 May	Phot	557.8	14.4.0
Grp25	NGC 3788	3247	2004 Dec	46 × 12	14.0.0	3247	2005 May	Phot	557.8	14.4.0
Grp26	NGC 3799	20140	2005 Dec	10 × 30	14.0.0	20140	2006 Jan	Phot	707.4	14.4.0
Grp26	NGC 3800	20140	2005 Dec	10 × 30	14.0.0	20140	2006 Jan	Phot	707.4	14.4.0
Grp27	IC 749	20140	2005 Dec	20 × 30	14.0.0	20140	2006 May	Phot	911.8	14.4.0

Table 2
(Continued)

GrpID (1)	Galaxy (2)	IRAC PID (3)	Date (4)	Exposure (5)	Pipeline (6)	MIPS PID (7)	Date (8)	Mode (9)	Exposure (10)	Pipeline (11)
Grp27	IC 750	20140	2005 Dec	20 × 30	14.0.0	20140	2006 May	Phot	911.8	14.4.0
Grp28	NGC 4038/4039	32	2003 Dec	100 × 12	13.2.0	32	2005 Jan	Scan	87.1	14.4.0
Grp29	NGC 4382	20140	2005 Dec	20 × 30	14.0.0	3649	2006 Jun	Phot	625	14.4.0
Grp29	NGC 4394	20140	2005 Dec	20 × 30	14.0.0	20140	2006 Jul	Phot	801.7	14.4.0
Grp30	NGC 4567	3247	2005 Jun	56 × 12	18.7.0	3247	2005 Jan	Phot	312.5	14.4.0
Grp30	NGC 4568	3247	2005 Jun	56 × 12	18.7.0	3247	2005 Jan	Phot	312.5	14.4.0
Grp31	NGC 4618	69	2004 May	10 × 30	13.2.0	69	2004 Jun	Phot	754.6	14.4.0
Grp31	NGC 4618	159	2004 May	16 × 30	13.2.0	159	2005 Dec	Scan	176.6	14.4.0
Grp31	NGC 4625	69	2004 May	10 × 30	13.2.0	69	2004 Jun	Phot	278.9	14.4.0
Grp31	NGC 4625	159	2004 May	16 × 30	13.2.0	159	2005 Dec	Scan	165.7	14.4.0
Grp32	NGC 4647	69	2004 Jun	10 × 12	13.2.0	69	2005 Jun	Phot	139.4	18.12.0
Grp32	NGC 4649	69	2004 Jun	10 × 12	13.2.0	69	2005 Jun	Phot	278.9	18.12.0
Grp33	NGC 4933A	20140	2006 Feb	20 × 30	14.0.0	20140	2006 Feb	Phot	707.4	14.4.0
Grp33	NGC 4933B	20140	2006 Feb	20 × 30	14.0.0	20140	2006 Feb	Phot	707.4	14.4.0
Grp33	NGC 4933C	20140	2006 Feb	20 × 30	14.0.0	20140	2006 Feb	Phot	707.4	14.4.0
Grp34	M51A	159	2004 May	108 × 30	13.2.0	159	2004 Jun	Scan	175.8	14.4.0
Grp34	M51B	159	2004 May	108 × 30	13.2.0	159	2004 Jun	Scan	174.5	14.4.0
Grp35	NGC 5350	50764	2008 Jun	32 × 30	18.18.0	20140	2006 Jun	Phot	707.4	14.4.0
Grp35	NGC 5353	69	2004 May	11 × 12	18.18.0	69	2005 May	Phot	165.7	14.4.0
Grp35	NGC 5353	50764	2008 Jun	32 × 30	18.18.0	20140	2006 Jun	Phot	707.4	14.4.0
Grp35	NGC 5354	69	2004 May	11 × 12	18.18.0	69	2005 May	Phot	165.7	14.4.0
Grp35	NGC 5354	50764	2008 Jun	32 × 30	18.18.0	20140	2006 Jun	Phot	707.4	14.4.0
Grp36	NGC 5394	3672	2005 Jan	10 × 30	18.7.0	3247	2005 Jan	Phot	557.8	14.4.0
Grp36	NGC 5395	3672	2005 Jan	10 × 30	18.7.0	3247	2005 Jan	Phot	557.8	14.4.0
Grp37	NGC 5457	60	2004 Mar	338 × 12	13.2.0	60	2007 Jun	Scan	176.5	14.4.0
Grp37	NGC 5474	159	2004 May	62 × 30	13.2.0	159	2004 Dec	Scan	162.1	18.12.0
Grp38	NGC 5426	3247	2005 Jul	72 × 12	13.2.0	2347	2004 Dec	Phot	312.5	14.4.0
Grp38	NGC 5427	3247	2005 Jul	72 × 12	13.2.0	3247	2005 Aug	Phot	312.5	14.4.0
Grp39	NGC 5480	20140	2005 Dec	20 × 30	14.0.0	20140	2006 Feb	Phot	728.4	14.4.0
Grp39	NGC 5481	20140	2005 Dec	20 × 30	14.0.0	20140	2006 Feb	Phot	728.4	14.4.0
Grp40	NGC 5544	20140	2006 Feb	10 × 30	14.0.0	20140	2006 Feb	Phot	372.0	14.4.0
Grp40	NGC 5545	20140	2006 Feb	10 × 30	14.0.0	20140	2006 Feb	Phot	372.0	14.4.0
Grp41	NGC 5614	20140	2006 Feb	10 × 30	14.0.0	20140	2006 Jun	Phot	712.6	14.4.0
Grp41	NGC 5615	20140	2006 Feb	10 × 30	14.0.0	20140	2006 Jun	Phot	712.6	14.4.0
Grp42	NGC 5846	20140	2006 Feb	20 × 30	14.0.0	69	2004 Feb	Phot	165.7	14.4.0
Grp42	NGC 5846A	20140	2006 Feb	20 × 30	14.0.0	69	2004 Feb	Phot	165.7	14.4.0
Grp42	NGC 5850	20140	2006 Feb	20 × 30	14.0.0	20140	2006 Mar	Phot	445.4	14.4.0
Grp43	NGC 5905	20140	2005 Dec	20 × 30	14.0.0	20140	2006 Mar	Phot	1168.5	14.4.0
Grp43	NGC 5908	20140	2005 Dec	20 × 30	14.0.0	20140	2006 Mar	Phot	1168.5	14.4.0
Grp44	NGC 5929	3269	2005 Jan	212 × 12	18.18.0	20140	2006 Mar	Phot	911.8	14.4.0
Grp44	NGC 5930	3269	2005 Jan	212 × 12	18.18.0	20140	2006 Mar	Phot	911.8	14.4.0
Grp45	NGC 5953	59	2004 Mar	8 × 12	13.2.0	59	2005 Aug	Phot	101.3	14.4.0
Grp45	NGC 5954	59	2004 Mar	8 × 12	13.2.0	59	2005 Aug	Phot	101.3	14.4.0
Grp46	NGC 5981	3403	2004 Dec	35 × 30	14.0.0	3403	2005 Jan	Phot	165.7	14.4.0
Grp46	NGC 5985	3403	2004 Dec	35 × 30	14.0.0	3403	2005 Jan	Phot	165.7	14.4.0
Grp47	Arp 314A	20140	2005 Nov	20 × 30	14.0.0	20140	2005 Nov	Phot	896.0	14.4.0
Grp47	Arp 314B	20140	2005 Nov	20 × 30	14.0.0	20140	2005 Nov	Phot	896.0	14.4.0
Grp47	Arp 314C	20140	2005 Nov	20 × 30	14.0.0	20140	2005 Nov	Phot	896.0	14.4.0
Grp48	NGC 7714	59	2004 Nov	8 × 12	13.2.0	59	2004 Dec	Phot	588.6	14.4.0
Grp48	NGC 7715	59	2004 Nov	8 × 12	13.2.0	59	2004 Dec	Phot	588.6	14.4.0

background mesh was selected to be larger than the galaxy structures but small enough to allow for small scale fluctuations in the images (individual group images were checked to ensure correct scales were selected for each system).

In many of the images the apertures from the individual galaxies were overlapping, a consequence of the close proximity of the galaxy isophotes. To correct for this, the MASK TYPE parameter CORRECT was selected. In cases where apertures overlapped, the pixel value in this region was discarded and replaced by a value symmetric about the galaxy's center. In most cases the overlap region is minimal and the difference between using either CORRECT or NONE (where the overlap region is included in both apertures) results in changes in flux that are within the flux calibration uncertainties. This masking parameter was also determined to provide the most reliable flux measurement for instances where the smaller galaxy aperture was completely contained within the larger aperture. In the case of Grp28 (NGC 4038/4039; The Antennae) the overlap region of the two galaxies contains enhanced emission arising from the interaction, and therefore

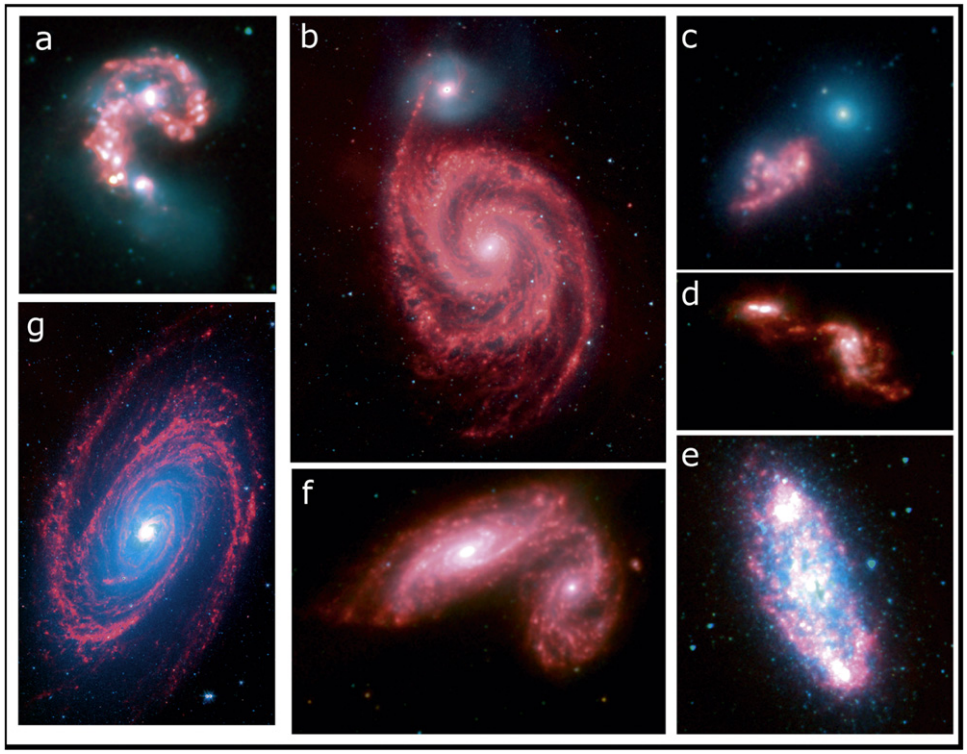

Figure 2. A composite three color image presenting seven examples of interacting systems in our sample. (a) Grp28, NGC 4038/4039 (The Antennae galaxy), (b) Grp34, NGC 5194/5195 (M51), (c) Grp1, NGC 274/275, (d) Grp21, NGC 3395/3396, (e) Grp16, NGC 2976, (f) Grp30, NGC4567/4568, and (g) NGC 3031, part of Grp17. In all frames the NS 8.0 μm emission is presented in red, 4.5 μm in green, and 3.6 μm in blue.

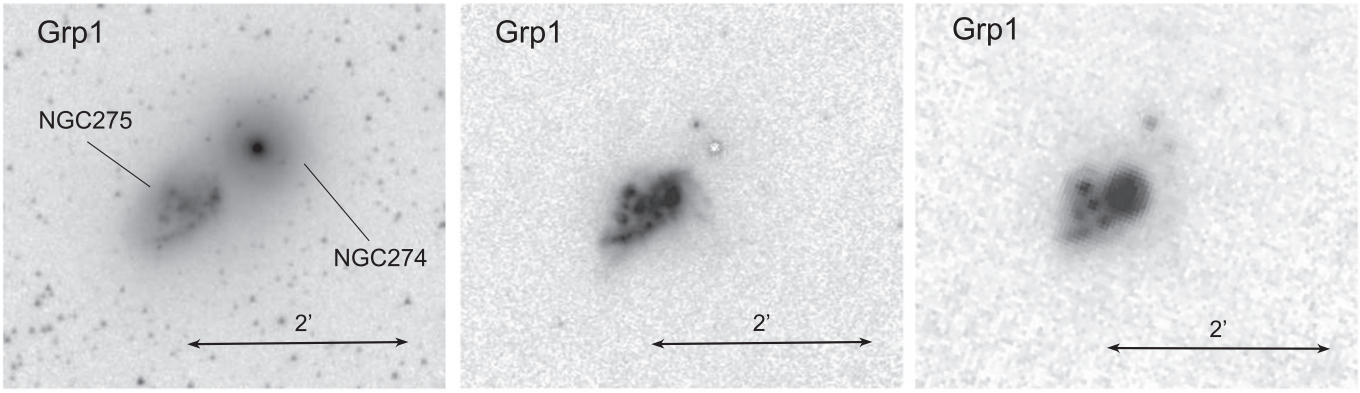

Figure 3. Grayscale negative images of the Grp 1 galaxies. The other 103 SIGS galaxies are available in the figure set in the electronic edition. From left, the three panels present the 3.6 μm, non-stellar 8 μm, and MIPS 24 μm, images, respectively. In the left panel galaxy names are also presented. Scale bars are shown in each panel.

(The complete figure set (63 images) is available.)

replacing the pixel values with a symmetric value results in an underestimation of flux. In this instance it was not possible to measure the individual galaxies' fluxes and therefore a combined value is presented for the whole system.

The parameters used for the majority of our photometry are presented in Table 3, and values that were altered for some of the more complicated systems are indicated. With these settings, foreground stars were also detected in the images and automatically removed from the integrated aperture fluxes. These values, defined as FLUX AUTO (based upon the Kron radius which is defined to measure 90% of an object's light; Kron 1980; Graham & Driver 2005), were extracted for each galaxy, and aperture corrections were applied to account for both the "extended" emission from the IRAC PSF itself and the diffuse scattering of the emission across the IRAC focal plane. The values for these corrections are provided in Table 4.7 of the IRAC Instrument Handbook.[11] Three of our galaxies (Grp23: UGC 6016, 5.8 μm; Grp39: NGC 5481, NS; Grp48: NGC 7715, 5.8 μm) had very low surface brightness in one band, therefore SExtrator was unable to provide fluxes for these individual bands, and upper limits are instead provided. These are defined to be 3 times the standard deviation of the background sky emission. All fluxes for the IRAC passbands are presented in Table 4 (alongside the MIPS 24 μm values, discussed in Section 3.2), and upper and lower limits are

[11] http://irsa.ipac.caltech.edu/data/SPITZER/docs/irac/iracinstrumenthandbook/

Table 3
Default SExtractor Photometry Parameters

Parameter	Value	Notes
DETECT_MINAREA	250	Minimum number of pixels above threshold. For some systems this was adjusted
FILTER	Y	...
FILTER_NAME	Gauss_2.5_5 × 5.conv	5 × 5 convolution mask of a Gaussian PSF with FWHM = 2.0 pixels
DEBLEND_NTHRESH	32	Number of deblending sub-thresholds. For some systems this was adjusted
DEBLEND_MINCONT	0.01	Minimum contrast parameter for deblending. For some systems this was adjusted
MASK_TYPE	CORRECT	Type of deblending. See Section 3.1 for more information
PHOT_AUTOPARAMS	2.5, 3.5	Kron_fact and min_radius
BACK_TYPE	AUTO	...
BACK_SIZE	128–768	Sized used to determine background. Varied depending on each system
BACKPHOTO_TYPE	GLOBAL	...
Photometry Output	FLUX_AUTO	Flexible elliptical aperture, defined by Kron radius (Kron 1980)

indicated. The uncertainties in the 3.6–8.0 μm flux densities are dominated by the cryogenic IRAC absolute flux calibration uncertainties (3%, 1σ).

3.2. MIPS Images

All MIPS data were reduced using standard techniques. We used object-masked median stacks of all exposures of each target to eliminate array artifacts from the enhanced BCD before mosaicking. The pre-processed data were then combined with MOPEX to mosaics with 2.″45 pixels. To perform aperture photometry on these galaxies, ensuring consistency between the derived fluxes and those from the IRAC images, SWarp was used to register the IRAC images to the same spatial scale as the MIPS images. The 2.″45 resolution 3.6 μm image was then used to define apertures in two image mode in SExtractor, using the same procedure as detailed in Section 3.1. From the apertures measured by SExtractor we applied appropriate aperture corrections, interpolating between the values provided in Table 4.14 of the MIPS Instrument Handbook. The 1σ MIPS uncertainties are estimated to be 8% and arise from the uncertainty in the absolute calibration. The 24 μm flux densities are presented in Table 4. In most cases the 2.″45 resolution defined apertures were larger than the 0.″6 resolution IRAC apertures, where elliptical radii were ∼10–20% larger. However, the flux densities derived from both the 0.″6 and 2.″5 resolution IRAC images are consistent ($\leqslant$10%) for all galaxies.

3.3. Saturation Corrections

For some of the galaxies in our sample, even the IRAC HDR frames exhibited saturation. For three galaxies; NGC 3034 (Grp17, M82) and IC 694 and NGC 3690 (Grp24), the 4.5, 5.8, 8.0 and 24 μm images were saturated. To address this, integrated photometry for NGC 3034 was adopted from Dale et al. (2009), who used the 1.2 s exposures to correct the IRAC derived photometry in cases of saturation and present 24 μm flux densities approximated from the *IRAS* data (via νf_ν (24 μm) = νf_ν (25 μm)); these values should be used with caution. For both galaxies in Grp24 the final mosaics were created from the 0.6 second BCD frames only. This provides reliable fluxes for the 3.6, 4.5 and 5.8 μm bands, but the 8.0 μm images were still saturated and are therefore presented as lower limits. The 24 μm values presented for these galaxies are also provided as lower limits. Three further galaxies exhibited saturation in the 8.0 μm images only, NGC 839 (Grp5), NGC 2633 (Grp11), and NGC 5394 (Grp36), and the flux densities provided for these galaxies are therefore lower limits.

3.4. Comparisons with the Literature

Twenty-eight of the galaxies in the SIGS sample have also been included in other large *Spitzer* surveys, notably the *Spitzer* Local Volume Legacy Survey (LVL; Dale et al. 2009) and the *Spitzer* Spirals, Bridges, and Tails Interacting Galaxy Survey (SB&T; Smith et al. 2007). We have compared our measured flux densities for these 28 galaxies with those determined from those surveys to investigate the additional uncertainties that may arise from the different techniques used in selecting photometry apertures.

The apertures from the SB&T survey were individually selected rectangular regions, chosen to separately determine the disk and tidal emission from each interacting system. From comparing the total flux densities from these regions (applying aperture corrections where necessary) to our global value provides flux densities that agree within 5–20% for the whole systems (except for Grp34, which we discuss below). For the LVL sample apertures are not provided, but all values differ by <15% except for NGC 3034 (Grp17). As discussed in Section 3.1, the MIR images are heavily saturated for this galaxy, therefore we adopt the corrected values presented by Dale et al. (2009). There are some differences between the flux densities provided in this paper and those presented by Lanz et al. (2013), where a multi-wavelength study of a subsample of SIGS is presented. In most instances these differences are <10%, but for some systems there are larger discrepancies. For these, either the aperture used by Lanz et al. (2013) was larger because the UV image was used to define the aperture size in cases of more extended UV emission, or the galaxies had flux density arising from overlapping regions and we have used a different correction method than Lanz et al. (2013), resulting in flux density differences between individual galaxies although the combined emission from these groups is consistent.

One system, Grp34, NGC 5194/5195, (=M51), is presented in both SB&T and LVL, as well as this paper and Lanz et al. (2013). Our derived values for the overall fluxes of the whole system are in agreement with the other values across all bands, apart from the 24 μm value from SB&T, which is 26–43% higher than the value presented in the other three papers. However, when comparing the flux from NGC 5194 (or NGC 5195) alone, the values show much greater range. This indicates that while the total fluxes presented in different survey papers are reliable, the treatment of overlapping regions can lead to significant flux differences for individual galaxies, and care should be taken to understand the treatment of flux in this situation.

Table 4
Spitzer Flux Densities for all SIGS Galaxies

GrpID (1)	Galaxy (2)	$f_{3.6\ \mu m}$ (mJy) (3)	$f_{4.5\ \mu m}$ (mJy) (4)	$f_{5.8\ \mu m}$ (mJy) (5)	$f_{8.0\ \mu m}$ (mJy) (6)	f_{NS} (mJy) (7)	$f_{24\ \mu m}$ (mJy) (8)
Grp1	NGC 274	57 ± 2	37 ± 1	23.8 ± 0.7	17.9 ± 0.5	6.5 ± 0.2	20 ± 2
Grp1	NGC 275	48 ± 1	34 ± 1	69 ± 2	171 ± 5	161 ± 5	430 ± 30
Grp2	NGC 470	107 ± 3	73 ± 2	144 ± 4	390 ± 10	370 ± 10	790 ± 60
Grp2	NGC 474	111 ± 3	69 ± 2	43 ± 1	25.4 ± 0.8	4.9 ± 0.1	12 ± 1
Grp3	NGC 520	171 ± 5	129 ± 4	309 ± 9	830 ± 20	800 ± 20	2400 ± 200
Grp4	IC 195	25.5 ± 0.8	16.1 ± 0.5	8.6 ± 0.3	5.6 ± 0.2	0.6 ± 0.0	2.0 ± 0.2
Grp4	IC 196	49 ± 1	31.2 ± 0.9	25.5 ± 0.8	41 ± 1	32 ± 1	41 ± 3
Grp5	NGC 833	48 ± 1	31.0 ± 0.9	20.5 ± 0.6	23.2 ± 0.7	13.5 ± 0.4	8.2 ± 0.7
Grp5	NGC 835	92 ± 3	64 ± 2	104 ± 3	276 ± 8	257 ± 8	190 ± 10
Grp5	NGC 838	68 ± 2	51 ± 2	178 ± 5	570 ± 20	550 ± 20	880 ± 70
Grp5	NGC 839	51 ± 2	44 ± 1	115 ± 3	>326	>316	1150 ± 90
Grp6	IC 1801	36 ± 1	24.7 ± 0.7	47 ± 1	125 ± 4	117 ± 4	160 ± 10
Grp6	NGC 935	74 ± 2	51 ± 2	100 ± 3	288 ± 9	273 ± 8	310 ± 30
Grp7	NGC 1241	117 ± 4	79 ± 2	120 ± 4	324 ± 10	302 ± 9	440 ± 40
Grp7	NGC 1242	10.7 ± 0.3	7.1 ± 0.2	18.5 ± 0.6	30.5 ± 0.9	28.5 ± 0.9	54 ± 4
Grp8	NGC 1253	87 ± 3	61 ± 2	65 ± 2	197 ± 6	181 ± 5	240 ± 20
Grp8	NGC 1253 A	11.4 ± 0.3	8.1 ± 0.2	5.8 ± 0.2	24.2 ± 0.7	22.1 ± 0.7	41 ± 3
Grp9	NGC 2276	150 ± 4	102 ± 3	312 ± 9	860 ± 30	830 ± 30	1400 ± 100
Grp10	NGC 2444	46 ± 1	28.9 ± 0.9	17.9 ± 0.5	12.4 ± 0.4	3.4 ± 0.1	10.2 ± 0.8
Grp10	NGC 2445	47 ± 1	32 ± 1	57 ± 2	158 ± 5	149 ± 4	410 ± 30
Grp11	NGC 2633	108 ± 3	78 ± 2	207 ± 6	>620	>600	2100 ± 200
Grp11	NGC 2634	79 ± 2	50 ± 1	29.1 ± 0.9	18.0 ± 0.5	2.6 ± 0.1	5.1 ± 0.4
Grp11	NGC 2634 A	9.0 ± 0.3	6.1 ± 0.2	7.0 ± 0.2	14.8 ± 0.4	13.1 ± 0.4	39 ± 3
Grp12	NGC 2719	8.2 ± 0.2	6.0 ± 0.2	7.7 ± 0.2	17.4 ± 0.5	15.8 ± 0.5	86 ± 7
Grp12	NGC 2719 A	3.7 ± 0.1	2.7 ± 0.1	3.8 ± 0.1	7.9 ± 0.2	7.2 ± 0.2	95 ± 8
Grp13	NGC 2805	64 ± 2	41 ± 1	57 ± 2	165 ± 5	153 ± 5	210 ± 20
Grp13	NGC 2814	14.2 ± 0.4	10.0 ± 0.3	17.5 ± 0.5	44 ± 1	41 ± 1	90 ± 7
Grp14	NGC 2820	52 ± 2	37 ± 1	79 ± 2	206 ± 6	195 ± 6	260 ± 20
Grp14	NGC 2820 A	2.8 ± 0.1	2.1 ± 0.1	2.0 ± 0.1	4.6 ± 0.1	4.1 ± 0.1	43 ± 3
Grp15	NGC 2964	173 ± 5	120 ± 4	258 ± 8	710 ± 20	680 ± 20	1300 ± 100
Grp15	NGC 2968	154 ± 5	94 ± 3	52 ± 2	38 ± 1	8.6 ± 0.3	17 ± 1
Grp15	NGC 2970	12.8 ± 0.4	8.3 ± 0.2	4.7 ± 0.1	3.9 ± 0.1	1.5 ± 0.1	4.6 ± 0.4
Grp16	NGC 2976	400 ± 10	270 ± 8	430 ± 10	960 ± 30	890 ± 30	1400 ± 100
Grp17	NGC 3031	10500 ± 300	6600 ± 200	5300 ± 200	6600 ± 200	4600 ± 100	5300 ± 400
Grp17	NGC 3034[a]	7300 ± 200	5800 ± 200	23700 ± 700	62200 ± 1900	60400 ± 1800	93200 ± 7500
Grp17	NGC 3077	420 ± 10	289 ± 9	299 ± 9	670 ± 20	600 ± 20	1600 ± 100
Grp18	NGC 3165	8.4 ± 0.3	5.8 ± 0.2	5.2 ± 0.2	10.5 ± 0.3	8.8 ± 0.3	14 ± 1
Grp18	NGC 3166	390 ± 10	256 ± 8	191 ± 6	249 ± 7	172 ± 5	230 ± 20
Grp18	NGC 3169	420 ± 10	272 ± 8	360 ± 10	830 ± 20	750 ± 20	600 ± 50
Grp19	NGC 3185	72 ± 2	47 ± 1	51 ± 2	115 ± 3	102 ± 3	180 ± 10
Grp19	NGC 3187	19.2 ± 0.6	13.4 ± 0.4	23.8 ± 0.7	57 ± 2	54 ± 2	84 ± 7
Grp19	NGC 3190	340 ± 10	216 ± 6	186 ± 6	288 ± 9	221 ± 7	260 ± 20
Grp20	NGC 3226	138 ± 4	86 ± 3	52 ± 2	45 ± 1	18.7 ± 0.6	2.9 ± 0.2
Grp20	NGC 3227	306 ± 9	232 ± 7	275 ± 8	610 ± 20	550 ± 20	1600 ± 100
Grp21	NGC 3395	55 ± 2	39 ± 1	97 ± 3	263 ± 8	91 ± 3	470 ± 40
Grp21	NGC 3396	40 ± 1	28.0 ± 0.8	65 ± 2	173 ± 5	60 ± 2	680 ± 50
Grp22	NGC 3424	102 ± 3	73 ± 2	157 ± 5	450 ± 10	430 ± 10	610 ± 50
Grp22	NGC 3430	106 ± 3	71 ± 2	129 ± 4	350 ± 10	330 ± 10	330 ± 30
Grp23	NGC 3448	63 ± 2	45 ± 1	79 ± 2	191 ± 6	178 ± 5	580 ± 50
Grp23	UGC 6016	2.2 ± 0.1	1.5 ± 0.1	<5.0	0.8 ± 0.0	0.4 ± 0.0	5.1 ± 0.4
Grp24	IC 694	136 ± 4	>138	>455	>1150	>1120	>8800
Grp24	NGC 3690	169 ± 5	>241	>480	>1100	>1070	>10100
Grp25	NGC 3786	66 ± 2	51 ± 2	59 ± 2	126 ± 4	113 ± 3	270 ± 20
Grp25	NGC 3788	67 ± 2	44 ± 1	58 ± 2	136 ± 4	123 ± 4	160 ± 10
Grp26	NGC 3799	12.7 ± 0.4	8.5 ± 0.3	11.9 ± 0.4	31.4 ± 0.9	28.9 ± 0.9	48 ± 4
Grp26	NGC 3800	69 ± 2	48 ± 1	98 ± 3	284 ± 9	270 ± 8	400 ± 30
Grp27	IC 749	50 ± 1	33 ± 1	58 ± 2	156 ± 5	146 ± 4	160 ± 10
Grp27	IC 750	223 ± 7	161 ± 5	360 ± 10	1020 ± 30	980 ± 30	1600 ± 100
Grp28	NGC 4038/4039	520 ± 20	360 ± 10	740 ± 20	1910 ± 60	1800 ± 50	5800 ± 500
Grp29	NGC 4382	990 ± 30	610 ± 20	380 ± 10	195 ± 6	25.2 ± 0.8	71 ± 6
Grp29	NGC 4394	193 ± 6	121 ± 4	102 ± 3	193 ± 6	152 ± 5	119 ± 10

Table 4
(Continued)

GrpID	Galaxy	$f_{3.6\ \mu m}$ (mJy)	$f_{4.5\ \mu m}$ (mJy)	$f_{5.8\ \mu m}$ (mJy)	$f_{8.0\ \mu m}$ (mJy)	f_{NS} (mJy)	$f_{24\ \mu m}$ (mJy)
Grp30	NGC 4567	165 ± 5	109 ± 3	172 ± 5	470 ± 10	440 ± 10	490 ± 40
Grp30	NGC 4568	360 ± 10	245 ± 7	480 ± 10	1340 ± 40	1270 ± 40	1600 ± 100
Grp31	NGC 4618	149 ± 4	100 ± 3	137 ± 4	302 ± 9	274 ± 8	370 ± 30
Grp31	NGC 4625	43 ± 1	28.4 ± 0.9	47 ± 1	120 ± 4	112 ± 3	130 ± 10
Grp32	NGC 4647	159 ± 5	102 ± 3	204 ± 6	530 ± 20	510 ± 20	550 ± 40
Grp32	NGC 4649	1330 ± 40	790 ± 20	460 ± 10	287 ± 9	39 ± 1	83 ± 7
Grp33	NGC 4933 A	24.2 ± 0.7	15.5 ± 0.5	8.5 ± 0.3	7.8 ± 0.2	2.9 ± 0.1	6.2 ± 0.5
Grp33	NGC 4933 B	116 ± 3	74 ± 2	48 ± 1	66 ± 2	43 ± 1	41 ± 3
Grp33	NGC 4933 C	6.1 ± 0.2	3.8 ± 0.1	1.3 ± 0.1	3.4 ± 0.1	2.6 ± 0.1	1.3 ± 0.1
Grp34	M51A	2690 ± 80	1790 ± 50	3900 ± 100	10500 ± 300	10000 ± 300	11400 ± 900
Grp34	M51B	940 ± 30	620 ± 20	570 ± 20	860 ± 30	680 ± 20	1400 ± 100
Grp35	NGC 5350	111 ± 3	62 ± 2	101 ± 3	244 ± 7	226 ± 7	380 ± 30
Grp35	NGC 5353	258 ± 8	158 ± 5	98 ± 3	60 ± 2	14.4 ± 0.4	27 ± 2
Grp35	NGC 5354	161 ± 5	98 ± 3	58 ± 2	33 ± 1	5.7 ± 0.2	8.2 ± 0.7
Grp36	NGC 5394	37 ± 1	26.4 ± 0.8	66 ± 2	>201	>192	870 ± 70
Grp36	NGC 5395	136 ± 4	89 ± 3	146 ± 4	390 ± 10	360 ± 10	420 ± 30
Grp37	NGC 5457	2650 ± 80	1520 ± 50	2520 ± 80	6900 ± 200	6400 ± 200	10000 ± 800
Grp37	NGC 5474	99 ± 3	65 ± 2	61 ± 2	100 ± 3	81 ± 2	150 ± 10
Grp38	NGC 5426	75 ± 2	52 ± 2	105 ± 3	292 ± 9	277 ± 8	320 ± 30
Grp38	NGC 5427	151 ± 5	107 ± 3	196 ± 6	560 ± 20	530 ± 20	740 ± 60
Grp39	NGC 5480	66 ± 2	46 ± 1	112 ± 3	328 ± 10	315 ± 9	370 ± 30
Grp39	NGC 5481	57 ± 2	35 ± 1	18.7 ± 0.6	8.3 ± 0.2	<0.9	5.1 ± 0.4
Grp40	NGC 5544	33 ± 1	18.1 ± 0.5	12.3 ± 0.4	15.8 ± 0.5	9.4 ± 0.3	13 ± 1
Grp40	NGC 5545	25.1 ± 0.8	15.4 ± 0.5	24.9 ± 0.7	65 ± 2	60 ± 2	70 ± 6
Grp41	NGC 5614	141 ± 4	84 ± 3	75 ± 2	143 ± 4	116 ± 3	116 ± 9
Grp41	NGC 5615	6.7 ± 0.2	4.2 ± 0.1	4.8 ± 0.1	11.7 ± 0.4	10.4 ± 0.3	39 ± 3
Grp42	NGC 5846	480 ± 10	287 ± 9	170 ± 5	104 ± 3	23.8 ± 0.7	22 ± 2
Grp42	NGC 5846 A	33 ± 1	20.3 ± 0.6	11.7 ± 0.4	7.7 ± 0.2	1.3 ± 0.1	2.6 ± 0.2
Grp42	NGC 5850	172 ± 5	104 ± 3	73 ± 2	164 ± 5	128 ± 4	119 ± 10
Grp43	NGC 5905	83 ± 2	55 ± 2	81 ± 2	232 ± 7	215 ± 6	330 ± 30
Grp43	NGC 5908	191 ± 6	131 ± 4	173 ± 5	410 ± 10	370 ± 10	440 ± 30
Grp44	NGC 5929	33 ± 1	22.1 ± 0.7	27.5 ± 0.8	43 ± 1	37 ± 1	123 ± 10
Grp44	NGC 5930	73 ± 2	49 ± 1	110 ± 3	271 ± 8	256 ± 8	1300 ± 100
Grp45	NGC 5953	84 ± 3	59 ± 2	132 ± 4	400 ± 10	380 ± 10	810 ± 60
Grp45	NGC 5954	42 ± 1	29.9 ± 0.9	71 ± 2	219 ± 7	211 ± 6	460 ± 40
Grp46	NGC 5981	66 ± 2	43 ± 1	39 ± 1	79 ± 2	66 ± 2	84 ± 7
Grp46	NGC 5985	182 ± 5	115 ± 3	117 ± 4	256 ± 8	221 ± 7	250 ± 20
Grp47	Arp314A	28.8 ± 0.9	20.6 ± 0.6	52 ± 2	158 ± 5	152 ± 5	480 ± 40
Grp47	Arp314B	14.2 ± 0.4	10.1 ± 0.3	21.4 ± 0.6	56 ± 2	53 ± 2	200 ± 20
Grp47	Arp314C	1.0 ± 0.0	0.6 ± 0.0	0.8 ± 0.0	1.0 ± 0.0	0.8 ± 0.0	2.3 ± 0.2
Grp48	NGC 7714	59 ± 2	43 ± 1	93 ± 3	297 ± 9	286 ± 9	2300 ± 200
Grp48	NGC 7715	5.9 ± 0.2	3.9 ± 0.1	<0.8	4.8 ± 0.1	3.7 ± 0.1	18 ± 1

Note. For IRAC photometry, 1 σ uncertainty is 3%, arising from the uncertainties in the cryogenic IRAC absolute flux calibration. MIPS uncertainties are 8%, again based on the absolute flux calibration. All values with upper and lower limits are discussed in Section 3.3, A a indicates fluxes were adopted from Dale et al. (2009, also discussed in Section 3.3).

In addition to the galaxies presented above, the MIR photometry for Grp5, or HCG 16, was presented by Johnson et al. (2007). All flux densities derived from the IRAC images presented by Johnson et al. (2007) are consistent with those presented in this paper. However, there are significant differences between the SIGS 24 μm flux densities. To investigate this discrepancy, we compared flux densities derived from fixed 7.″0 circular regions to those presented in a follow-up paper of the nuclear emission within Hickson Compact Groups (Gallagher et al. 2008) and determined that all fixed aperture 24 μm values are, within the uncertainties, consistent with Gallagher et al. (2008). This suggests that our differences in global 24 μm fluxes to Johnson et al. (2007) arise from the different treatment of overlapping apertures, where we have attributed flux in these regions using the CORRECT masking parameter from SExtractor.

3.5. Non-interacting Spirals Sample

To determine the level of enhanced activity in the SIGS galaxies relative to undisturbed spiral systems, we have used two control samples to compare with our galaxies. The first is a small subset of the normal galaxies presented by Smith et al. (2007), who used the *Spitzer* Infrared Nearby Galaxies Survey (SINGS; Kennicutt et al. 2003) to determine a sample of galaxies that are not subject to strong perturbing forces, although the galaxies could have distant or low-mass

Table 5
Basic Properties of SINGS Control Galaxies

Galaxy	Morphological Classification	Distance (Mpc)	Log(M) ($M_\odot$)
NGC 925	SABd	10.1	9.83
NGC 1291	SBa	9.7	10.77
NGC 2403	SABcd	3.5	9.66
NGC 2841	SAb	9.8	10.52
NGC 3049	SBab	19.6	9.45
NGC 3184	SABcd	8.6	9.96
NGC 3521	SABbc	9.0	10.68
NGC 3621	Sad	6.2	9.92
NGC 3938	SAc	12.2	10.04
NGC 4236	SBdm	3.5	8.62
NGC 4559	SABcd	11.6	10.03
NGC 4594	SAa	13.7	11.45
NGC 4736	SAab	5.3	10.42
NGC 4826	SAab	5.6	10.30
NGC 5055	SAbc	8.2	10.66
NGC 6946	SABcd	5.5	10.42

companions. This results in 26 spiral galaxies, but we exclude 10 galaxies that are associated with cluster or radial-velocity groups, resulting in 16 well isolated spirals. These are presented in Table 5. The photometry for this sample is taken from Dale et al. (2005) and the distances from Smith et al. (2007).[12] The galaxies in this sample have a maximum distance of 19.6 Mpc and a mass range from 4.2×10^8 to $2.8 \times 10^{11}\ M_\odot$.

Due to the limited size of the SINGS sample, we have combined this with a second control sample to provide a stronger statistical comparison, albeit with a larger range in distances. This second sample has been taken from Xu et al. (2010, their Table 4) and contains 38 isolated spiral galaxies that were selected to match the properties of the pair sample presented in that paper. These systems were selected from two *Spitzer* archive tables: the SWIRE survey of the Lockman field and ELAIS-N1 field (Lonsdale et al. 2003) and the SINGS sample (four galaxies are within both the SINGS sample and the Xu sample). Galaxy distances were calculated following the same method used for our sample (see Section 2) and range from 3.5 to ~300 Mpc. Combining these two samples provides us with a control sample of 50 isolated spiral galaxies.

4. MIR PROPERTIES

4.1. IR Colors

Figure 4 presents color–color plots for all SIGS galaxies. There is a trend of increasing [4.5]–[5.8] and [5.8]–[8.0] color as dust emission increases with galaxies populating the top right corner showing higher PAH emission and hence higher SFRs. The majority of these systems are classified as spiral galaxies (see Table 1 for morphological classifications) with some irregular galaxies also indicating higher SFR. The early-type systems are distinct from the spiral galaxies, lying toward the lower left corner of the plot, indicating lower levels of SFR. This behavior is also observed in the right hand panel, where the early-type galaxies exhibit lower 8.0 and 24 μm band emission (which are dominated by emission from both the 7.7 and 8.6 μm PAH features and warm dust grains, respectively) compared to the irregular and spiral galaxies. Further, the irregular galaxies exhibit much greater scatter than the other morphological classes as well as having redder [8.0]–[24.0] values. The Complete and Arp samples have galaxies that exhibit similar colors.

The isolated spiral galaxies from the control sample exhibit colors similar to those of the interacting spirals, although the interacting systems seem to have slightly redder [NS]–[24] values compared to the control sample, as the NS contribution rises relative to the stars. Due to the differences in properties of the early-type systems compared with the late-type systems (which have been noted in previous studies, e.g., Bendo et al. 2007; Young et al. 2009), when comparing SIGS to the control samples of isolated spiral galaxies it is more appropriate to include only the late-type systems. Further, the differences in colors of the irregular galaxies to those of spirals also indicates that these systems should be excluded in subsequent comparisons to allow us to study the effects of interactions on triggered SF in spiral galaxies. Irregular galaxies exhibit diverse properties and different modes of SF compared to spiral galaxies (continuous versus bursty, e.g., Hunter & Elmegreen 2004) and we have too few of these galaxies within SIGS to provide an adequate statistical sample. There are 17 early-type galaxies and 14 systems classed as irregulars in the SIGS sample. We have removed these galaxies, resulting in 72 spirals galaxies within the SIGS sample (24 within the Arp sample and the remaining 48 within the Complete sample).

In addition to including only spiral galaxies in our subsequent analysis, we have also used *Spitzer* colors to identify active galactic nucleus (AGN) activity. Figure 5 plots the IRAC colors for our sources in the Stern et al. (2005) AGN selection diagram. In the SIGS sample, 30 galaxies have been identified as hosting an AGN based on visible line-ratio diagnostics (K85; Ho et al. 1997), but only two galaxies have MIR colors implying AGN activity. There is some scatter in the low [3.6]–[4.5] values, consistent with the scatter observed in other large MIR star-forming galaxy surveys (e.g., Ashby et al. 2011).

The two galaxies located in and close to the Stern wedge are both members of Grp24; NGC 3690 and IC 694. Spectral mapping of these galaxies with the IR Spectrograph instrument onboard *Spitzer* (Alonso-Herrero et al. 2009) determined that NGC 3690 exhibits emission consistent with an AGN surrounded by a star-forming region. IC 694 (which has colors just outside the Stern region) has MIR emission characteristic of strong SF. Subsequent very long baseline interferometry (VLBI) radio observations at 1.7 and 5.0 GHz (Pérez-Torres et al. 2010) indicated the presence of an AGN in this system, which has recently been confirmed with high spatial resolution MIR spectroscopy (Alonso-Herrero et al. 2013). Therefore, due to the MIR colors presented in Figure 5, coupled with the evidence for an AGN provided in the literature, we exclude these two galaxies from all subsequent analysis of our sample's behavior with respect to SF.

The AGN contribution was investigated by Lanz et al. (2013), using the DECOMPIR tool (Mullaney et al. 2011) to estimate the contribution of AGN activity in the 8–35 μm emission of 9 SIGS galaxies (out of 35 studied). This analysis

[12] The published distances are in agreement with the values we determined using the method outlined in Section 2.

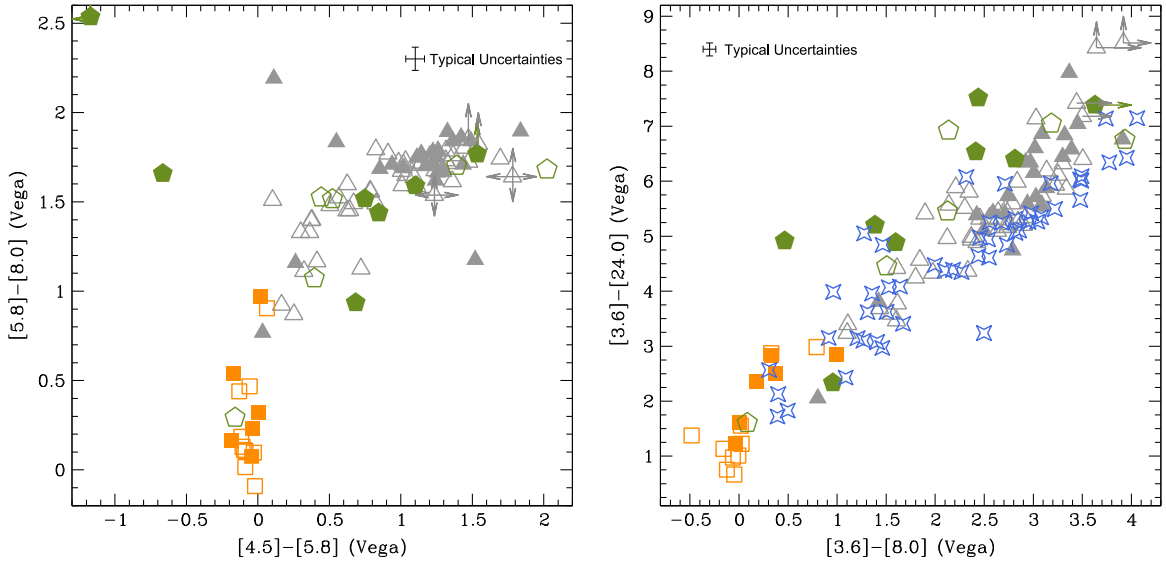

Figure 4. Color–color diagram for the SIGS galaxies; [4.5]–[5.8] vs. [5.8]–[8.0] and [3.6]–[8.0] vs. [8.0]–[24.0], are plotted left to right. Triangles indicate spiral galaxies, squares are early-type systems, and pentagons indicate irregular galaxies. All objects in the "Complete" sub-sample are plotted as open points and galaxies in the "Arp" sub-sample are filled. In the right panel the colors from the control sample are presented as blue stars. Arrows indicate cases where sources have only upper-limits (or lower-limits in the case of saturation) UGC 6061 (in Grp23), is outside of the color range of the left panel.

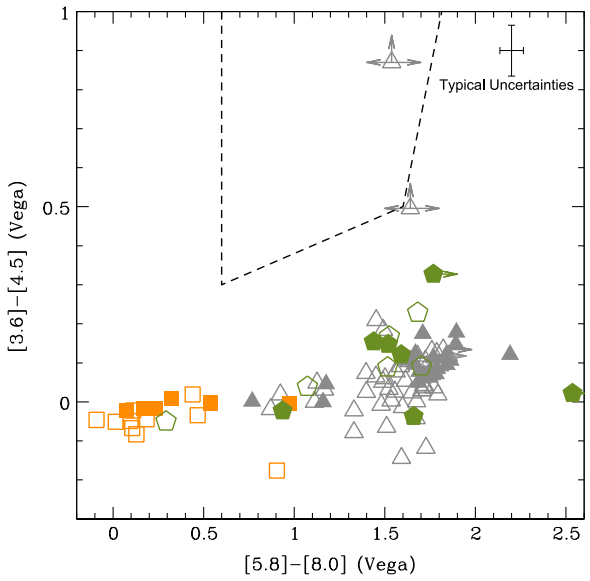

Figure 5. [5.8]–[8.0] vs. [3.6]–[4.5] color diagram. Symbols indicate both morphological type (gray triangles are spiral systems, orange squares are early-type galaxies, and green pentagons are irregular galaxies) and sub-samples (Complete open points, Arp filled points). Sources within the region indicated by the dashed line are AGN dominated in MIR emission (Stern et al. 2005).

showed that the total AGN contribution is at most 10% for most galaxies but indicated a higher contribution for NGC 3786 (Grp25) and NGC 3227 (Grp20), although the DECOMPIR fits for these galaxies were poor. Both of these systems, while exhibiting redder [3.6]–[4.5] colors than the majority of our sample (0.21 and 0.18 compared to a median value of 0.05 and upper quartile value of 0.11), are still both located well outside of the Stern wedge. We therefore include both systems in the following sections, but excluding these galaxies would not alter our conclusions.

4.2. Masses and sSFR

In Table 6 the monochromatic luminosities (νL_ν) for the 3.6 μm ($L(3.6)$), NS ($L(\mathrm{NS})$), and 24 μm ($L(24)$) are presented for the whole SIGS sample, alongside derived masses and sSFR for each galaxy. The stellar masses have been derived from the 3.6 μm photometry using the nonlinear relation presented by Zhu et al. (2010),

$$\log\left(\frac{M}{M_\odot}\right) = (-0.79 \pm 0.03) + (1.19 \pm 0.01) \times \log\left(\frac{L(3.6)}{L_\odot}\right). \quad (1)$$

We use this relation in preference to their color-corrected formula, which corrects for variations in the mass-to-light ratio, a consequence of different SF histories, as we do not have ($g - r$) colors for our whole sample. This will not significantly alter our masses, as shown by Bonfini (2013), who estimated that the maximum variation of the mass-to-light ratio between galaxies dominated by early and late-type stellar populations is ~30% (0.11 dex).

Figure 6 presents the distribution of masses for the SIGS sample. The whole SIGS sample and the spiral galaxies subset have similar distributions (which is expected, as the full sample predominantly contains spiral galaxies). The spiral galaxies sample contains systems ranging in masses from $\sim 10^8$ to $\sim 10^{11}\,M_\odot$ with most galaxies having masses $\sim 10^{10}\,M_\odot$. The Complete and Arp samples exhibit similar distributions. Galaxy mass ratios for each system are presented in Figure 7. For systems with more than two galaxies, the mass ratios are defined in the same manner as the separation values presented

Table 6
Derived Physical Properties for all SIGS Galaxies

GrpID	Galaxy	Log $\nu L_{\nu(3.6\,\mu m)}$ (erg s^{-1})	Log $\nu L_{\nu(NS)}$ (erg s^{-1})	Log $\nu L_{\nu(24\,\mu m)}$ (erg s^{-1})	Log (M) ($M_{\odot}$)	Log (sSFR) (yr^{-1})
(1)	(2)	(3)	(4)	(5)	(6)	(7)
Grp1	NGC 274	42.34	41.05	41.06	9.63	−11.27
Grp1	NGC 275	42.37	42.55	42.49	9.67	−9.87
Grp2	NGC 470	43.15	43.34	43.20	10.60	−10.09
Grp2	NGC 474	43.07	41.37	41.30	10.50	−11.89
Grp3	NGC 520	43.13	43.45	43.44	10.56	−9.81
Grp4	IC 195	42.79	40.85	40.86	10.17	−12.00
Grp4	IC 196	43.07	42.54	42.18	10.50	−11.01
Grp5	NGC 833	43.12	42.22	41.52	10.56	−11.72
Grp5	NGC 835	43.45	43.55	42.93	10.95	−10.71
Grp5	NGC 838	43.26	43.83	43.55	10.73	−9.87
Grp5	NGC 839	43.14	>43.59	43.68	10.58	−9.60
Grp6	IC 1801	43.03	43.20	42.85	10.45	−10.29
Grp6	NGC 935	43.37	43.59	43.17	10.85	−10.37
Grp7	NGC 1241	43.52	43.59	43.27	11.04	−10.46
Grp7	NGC 1242	42.48	42.56	42.36	9.80	−10.13
Grp8	NGC 1253	42.58	42.56	42.21	9.92	−10.40
Grp8	NGC 1253 A	41.83	41.77	41.57	9.02	−10.15
Grp9	NGC 2276	43.31	43.71	43.45	10.79	−10.02
Grp10	NGC 2444	43.21	41.73	41.73	10.66	−11.62
Grp10	NGC 2445	43.21	43.36	43.33	10.66	−10.02
Grp11	NGC 2633	43.08	>43.48	43.54	10.51	−9.67
Grp11	NGC 2634	42.93	41.10	40.92	10.33	−12.10
Grp11	NGC 2634 A	42.03	41.85	41.84	9.26	−10.11
Grp12	NGC 2719	42.32	42.25	42.51	9.60	−9.78
Grp12	NGC 2719 A	41.94	41.89	42.53	9.15	−9.31
Grp13	NGC 2805	42.70	42.74	42.41	10.06	−10.35
Grp13	NGC 2814	42.03	42.14	42.00	9.26	−9.94
Grp14	NGC 2820	42.56	42.78	42.43	9.89	−10.15
Grp14	NGC 2820 A	41.24	41.06	41.59	8.32	−9.42
Grp15	NGC 2964	42.92	43.17	42.98	10.32	−10.03
Grp15	NGC 2968	43.01	41.42	41.24	10.43	−11.89
Grp15	NGC 2970	41.96	40.70	40.69	9.18	−11.18
Grp16	NGC 2976	41.75	41.75	41.47	8.93	−10.15
Grp17	NGC 3031	43.18	42.47	42.06	10.63	−11.26
Grp17	NGC 3034	43.05	43.62	43.33	10.47	−9.83
Grp17	NGC 3077	41.81	41.63	41.58	9.00	−10.12
Grp18	NGC 3165	41.72	41.39	41.13	8.89	−10.45
Grp18	NGC 3166	43.28	42.58	42.22	10.75	−11.21
Grp18	NGC 3169	43.22	43.12	42.55	10.68	−10.82
Grp19	NGC 3185	42.57	42.37	42.14	9.90	−10.45
Grp19	NGC 3187	42.12	42.22	41.94	9.37	−10.12
Grp19	NGC 3190	43.24	42.71	42.29	10.70	−11.09
Grp20	NGC 3226	42.89	41.67	40.39	10.28	−12.52
Grp20	NGC 3227	43.12	43.02	43.02	10.56	−10.22
Grp21	NGC 3395	42.63	42.51	42.74	9.98	−9.92
Grp21	NGC 3396	42.50	42.33	42.90	9.81	−9.61
Grp22	NGC 3424	42.84	43.13	42.80	10.23	−10.12
Grp22	NGC 3430	42.88	43.03	42.55	10.28	−10.42
Grp23	NGC 3448	42.58	42.69	42.72	9.91	−9.88
Grp23	UGC 6016	41.20	40.12	40.75	8.28	−10.21
Grp24	IC 694	43.48	>44.05	>44.47	10.99	>-9.17
Grp24	NGC 3690	43.58	>44.03	>44.53	11.10	>-9.22
Grp25	NGC 3786	43.06	42.95	42.85	10.49	−10.33
Grp25	NGC 3788	42.96	42.87	42.51	10.36	−10.54
Grp26	NGC 3799	42.56	42.57	42.31	9.89	−10.27
Grp26	NGC 3800	43.30	43.54	43.23	10.77	−10.23
Grp27	IC 749	42.16	42.28	41.85	9.42	−10.26
Grp27	IC 750	43.09	43.38	43.12	10.52	−10.09
Grp28	NGC 4038/4039	43.53	43.73	43.75	11.05	−9.98
Grp29	NGC 4382	43.50	41.56	41.54	11.01	−12.15
Grp29	NGC 4394	42.74	42.29	41.71	10.11	−11.09

Table 6
(Continued)

GrpID	Galaxy	Log $\nu L_{\nu(3.6\,\mu m)}$ (erg s^{-1})	Log $\nu L_{\nu(NS)}$ (erg s^{-1})	Log $\nu L_{\nu(24\,\mu m)}$ (erg s^{-1})	Log (M) ($M_{\odot}$)	Log (sSFR) (yr^{-1})
(1)	(2)	(3)	(4)	(5)	(6)	(7)
Grp30	NGC 4567	42.67	42.75	42.32	10.03	−10.39
Grp30	NGC 4568	43.01	43.21	42.84	10.43	−10.28
Grp31	NGC 4618	41.83	41.75	41.41	9.02	−10.31
Grp31	NGC 4625	41.47	41.53	41.12	8.60	−10.17
Grp32	NGC 4647	42.66	42.82	42.38	10.01	−10.32
Grp32	NGC 4649	43.61	41.72	41.58	11.14	−12.22
Grp33	NGC 4933 A	42.75	41.49	41.33	10.12	−11.47
Grp33	NGC 4933 B	43.46	42.69	42.19	10.97	−11.47
Grp33	NGC 4933 C	42.16	41.43	40.67	9.41	−11.43
Grp34	M51A	43.21	43.43	43.01	10.66	−10.34
Grp34	M51B	42.75	42.26	42.11	10.11	−10.69
Grp35	NGC 5350	43.21	43.17	42.91	10.66	−10.44
Grp35	NGC 5353	43.57	41.97	41.78	11.10	−12.00
Grp35	NGC 5354	43.46	41.66	41.34	10.96	−12.30
Grp36	NGC 5394	43.08	>43.44	43.63	10.51	−9.57
Grp36	NGC 5395	43.64	43.72	43.31	11.18	−10.56
Grp37	NGC 5457	43.08	43.12	42.84	10.51	−10.37
Grp37	NGC 5474	41.55	41.11	40.90	8.69	−10.48
Grp38	NGC 5426	42.99	43.21	42.79	10.40	−10.30
Grp38	NGC 5427	43.35	43.55	43.21	10.83	−10.30
Grp39	NGC 5480	42.84	43.17	42.76	10.22	−10.15
Grp39	NGC 5481	42.86	40.72	41.00	10.25	−11.96
Grp40	NGC 5544	42.95	42.05	41.73	10.36	−11.32
Grp40	NGC 5545	42.84	42.87	42.46	10.22	−10.45
Grp41	NGC 5614	43.74	43.31	42.83	11.30	−11.15
Grp41	NGC 5615	42.43	42.28	42.37	9.74	−10.06
Grp42	NGC 5846	43.48	41.83	41.33	10.98	−12.30
Grp42	NGC 5846 A	42.32	40.55	40.39	9.60	−11.89
Grp42	NGC 5850	43.15	42.67	42.17	10.59	−11.11
Grp43	NGC 5905	43.39	43.46	43.16	10.88	−10.40
Grp43	NGC 5908	43.73	43.67	43.27	11.28	−10.71
Grp44	NGC 5929	42.70	42.40	42.44	10.05	−10.30
Grp44	NGC 5930	43.11	43.31	43.55	10.55	−9.69
Grp45	NGC 5953	42.97	43.28	43.13	10.38	−9.94
Grp45	NGC 5954	42.64	43.00	42.86	9.99	−9.82
Grp46	NGC 5981	42.76	42.41	42.04	10.13	−10.78
Grp46	NGC 5985	43.45	43.19	42.77	10.95	−10.88
Grp47	Arp 314 A	42.89	43.27	43.29	10.28	−9.68
Grp47	Arp 314 B	42.58	42.81	42.91	9.92	−9.70
Grp47	Arp 314 C	41.44	41.01	40.97	8.56	−10.27
Grp48	NGC 7714	42.90	43.25	43.68	10.30	−9.31
Grp48	NGC 7715	41.90	41.35	41.56	9.10	−10.23

in Table 1, where the most massive group members are selected as the dominant pair in the system, and smaller galaxy member mass ratios are calculated based on their nearest massive neighbor (see Section 2 for more details). Our sample contains a wide variety of mass ratio encounters ranging from major mergers, which we define to be all galaxies with mass ratios <1:4, through minor mergers, where mass ratios are >1:10. Our sample also contains a number of systems that fall into the "intermediate" mass ratios range (Bournaud et al. 2004).

Figure 8 presents the mass distribution of the SIGS spirals compared to the control sample. To ensure a fair comparison of sSFR enhancement between the two samples, it is important to check that they have similar mass ranges. The two samples exhibit similar distributions and therefore will not bias our sSFR comparisons. We used a Kolmogorov–Smirnov (KS) test to compare the two populations, which gives a null hypothesis rejection probability of 0.25, consistent with the two distributions coming from the same parent population.

The sSFRs in Table 6 have been derived using a monochromatic SFR relation based on the $L(24)$ emission. This correlation has been studied on both the local (spatial scale ~500 pc; Alonso-Herrero et al. 2006; Calzetti et al. 2007; Murphy et al. 2011) and global scales (Wu et al. 2005; Zhu et al. 2008; Kennicutt et al. 2009; Rieke et al. 2009), determining that all global linear calibrations are within 30% (Calzetti et al. 2010). Here we use the relations derived by

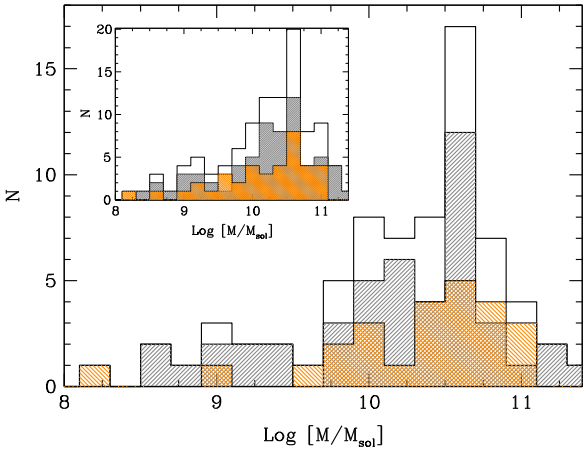

Figure 6. Histogram of the stellar mass distribution of all SIGS spirals (indicated by the open histogram). The inset plot presents the mass distribution of all 103 galaxies. In both plots the "Complete" (gray) and "Arp" (orange) samples are also shown.

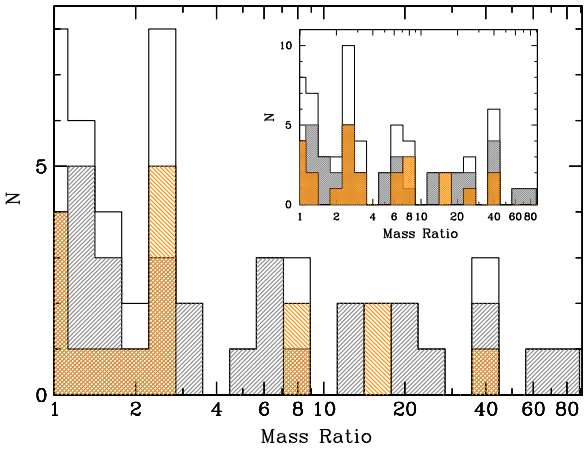

Figure 7. Histogram of the stellar mass ratios of the spiral galaxies (indicated by the open histogram). The inset plot presents the mass ratio distribution of all 103 galaxies. Colors show "Complete" (gray) and "Arp" (orange) samples.

Rieke et al. (2009)

$$\begin{aligned}\mathrm{SFR}(24) &= 2.04 \times 10^{-43} \times L(24), \left(L(24) < 5 \times 10^{43}\right) \\ &= 2.04 \times 10^{-43} \times L(24) \\ &\quad \times \left[2.03 \times 10^{-44} \times L(24)\right]^{0.048}, \\ &\quad \left(L(24) > 5 \times 10^{43}\right) \end{aligned} \quad (2)$$

where a small correction term for self-absorption is included for the high luminosity galaxies.[13] These SFR estimates are then normalized by the stellar mass of the galaxy to give a total sSFR for each galaxy. Lanz et al. (2013) reviewed the accuracy of these single-parameter formulae for estimating SFR.

5. SSFR ENHANCEMENT

The distribution of the sSFR of all galaxies, divided into morphological classes, is presented in Figure 9. Nearly all galaxies with log (sSFR) < -11.0 are early-type systems, while the irregular galaxies have a range of sSFR values. The properties of these early-type galaxies will be discussed in detail elsewhere.

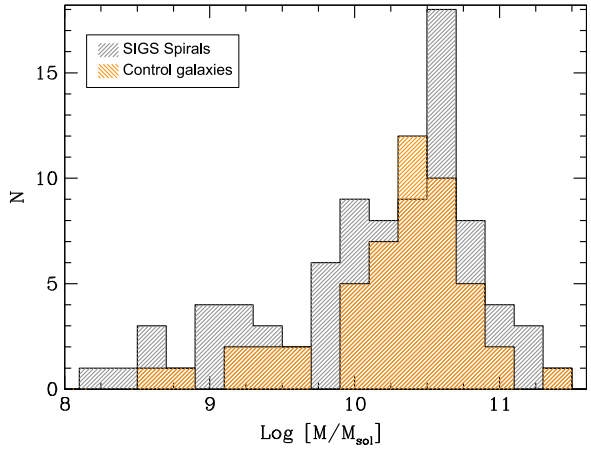

Figure 8. Histogram presenting the mass distribution of the SIGS spirals galaxies (gray) compared to the control sample (orange). Masses derived from the 3.6 μm flux densities (Equation (1)).

The median value of log (sSFR) for the whole SIGS sample is −10.32 (excluding both galaxies in Grp24, as discussed in Section 4.1) or −10.30 including only the spiral galaxies. From the flux densities presented in the SINGS and Xu samples we derived sSFRs (using Equation (2)) for all control galaxies. Masses were calculated using Equation (1), where [3.6] fluxes for the Xu sample were determined from the K_s values (presented in their Table 4), applying a constant of −0.32 mags.[14] The control sample has a median log (sSFR) value of −10.48 indicating some enhancement in our sample with respect to isolated field spirals. As discussed in Section 4.2, these differences do not arise from a mismatch in the mass distribution between the SIGS spiral sample and the control sample, which has a median mass value of $(2.7 \pm 0.4) \times 10^{10}$ $M_\odot$ compared to $(2.0 \pm 0.4) \times 10^{10}$ $M_\odot$ for the spiral SIGS galaxies. The sSFR distribution of the control sample compared to the sSFR distribution of the SIGS spirals is presented in Figure 10. Using the KS test we compared our spiral sample to the control population, determining a null hypothesis rejection significance of 2.4×10^{-3}, indicating with strong statistical significance that the two samples do not arise from the same parent populations.

Figure 11 shows the distribution of log (sSFR) of our spiral sample, divided into their Arp and Complete classifications. The two samples have similar overall distributions, but there are more galaxies with lower sSFR in the Complete sample, and the Arp sample contains a larger number of higher sSFR galaxies. This is also seen when comparing the median value of log (sSFR) for the two samples; −10.14 from the Arp galaxies compared to −10.33 for the Complete sample. We used the KS test to compare the two distributions, which resulted in a null hypothesis probability of 0.07, consistent with the samples arising from the same population. We further compared the populations using the Wilcoxon–Mann–Whitney (WMW) test, which is sensitive to differences in the median value of the samples as well as the shape of the distributions (Mann & Whitney 1947). Under the assumption that the Arp sample, which includes more obviously interacting galaxies, has a

[13] For the less massive and gas-poor galaxies (i.e., early-types), the monochromatic $L(24)$ calibration becomes uncertain, and tracers of both dust-obscured and unobscured SFR provide a more reliable value.

[14] We determined this constant by comparing [3.6] magnitudes and K_s magnitudes of >200 star-forming galaxies in the LVL survey (Dale et al. 2009).

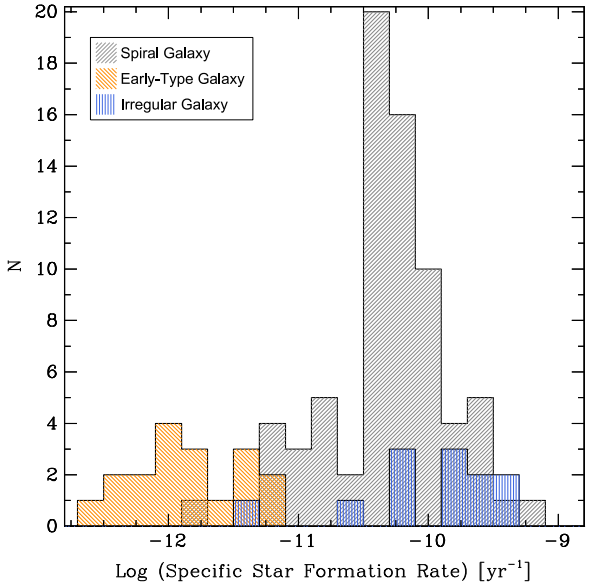

Figure 9. Histogram of the specific star formation rate (sSFR). SFR was derived from the 24 μm flux densities (Equation (2)) and mass from the 3.6 μm flux densities (Equation (1)). Histograms indicate spiral (gray), irregular (blue), and early-type (orange) galaxies.

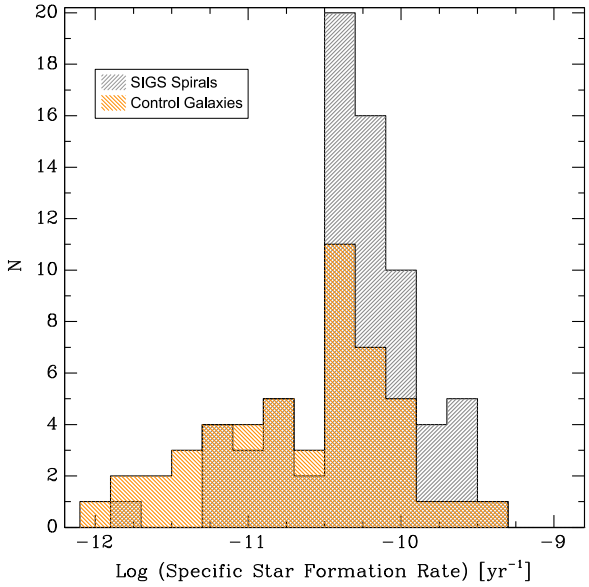

Figure 10. Histogram of sSFR from both the SIGS spirals (gray) and control sample (orange).

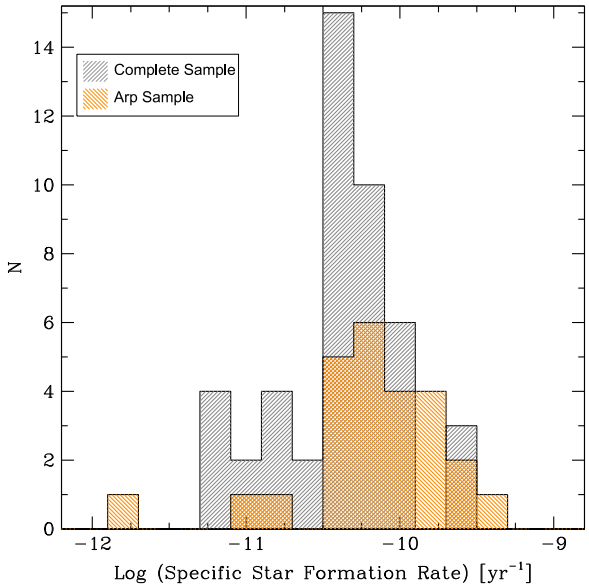

Figure 11. Histograms of the specific star formation rate distribution of the spiral galaxies from the "Complete" (gray) and "Arp" samples (orange).

higher median value (as we have shown above), we performed a one-tailed test, which resulted in a null hypothesis probability of 0.01, indicating marginal significance that the two sample do not arise from the same parent population. Comparing these two distributions to the control sample indicates statistically that neither arises from the same parent population as the isolated galaxies; the Complete sample has null hypotheses rejection probability of 0.02 and 0.01 for the KS test and WMW test respectively, and the Arp sample has probabilities of 4×10^{-4} and 3×10^{-4} (KS test and WMW test). In summary, these comparisons suggest that the SIGS spiral galaxy population has enhanced sSFR above field spiral galaxies. While the difference is most obvious for the Arp sample, even the Complete sample shows evidence for sSFR enhancement.

In our subsequent analysis and discussion we will focus on the spiral galaxy sample.

5.1. Evolution of sSFR During Interactions

To further probe the change in sSFR between different interactions, we use a morphology-based parameter that characterizes the strength of an encounter, which we term "interaction strength" (defined in Section 2 and presented in column 8 of Table 1). From this classification there are 21 Stage 2 spirals (35 galaxies in total including the early-type and irregular systems), 26 Stage 3 (34 in the overall sample), and 22 Stage 4 (31 in the overall sample). In addition there is also 1 Stage 5 system, NGC 520, which we do not use in the comparison between different stages. The sSFR distributions for these stages are shown in Figure 12. Somewhat surprising, given that we expect the Stage 4 systems to contain more evolved interactions, is the presence of systems with low sSFR in this stage. These galaxies are NGC 833 (Grp5), which is a member of HCG 16, and as such will be undergoing complex orbital dynamics which will influence the level of SF in the galaxy. The next lowest sSFR system is NGC 5614 (Grp41), a minor merger system with a mass ratio of 1:35, where NGC 5614 is the more massive galaxy.

The sSFR distribution of the Stage 4 galaxies extends to higher values than the earlier stages. This is reflected in the median sSFR of the sub-samples which are −10.26, −10.35, and −10.04, for stages 2, 3, and 4, respectively, where the values from stages 2 and 3 are consistent within uncertainties (S2: $(0.55 \pm 0.15) \times 10^{-10}\,\mathrm{yr}^{-1}$, S3:$(0.44 \pm 0.04) \times 10^{-10}\,\mathrm{yr}^{-1}$, see Table 7). The KS test and WMW test find no statistical difference between the sSFR distribution of the Stage 2 and Stage 3 systems. The Stage 3 and Stage 4 galaxies do not arise from the same parent population (null hypothesis probabilities of 0.003 and 0.004 for the KS test and WMW test, respectively). The stages 2 and 4 distributions are not distinguishable (null hypothesis probabilities of 0.09 and 0.03 for the KS test and WMW test, respectively). Using both the KS test and WMW test to compare the sSFR in each of the three stages to the control sample strongly indicates that Stages 3 and 4 do not arise from the same population, and Stage 2

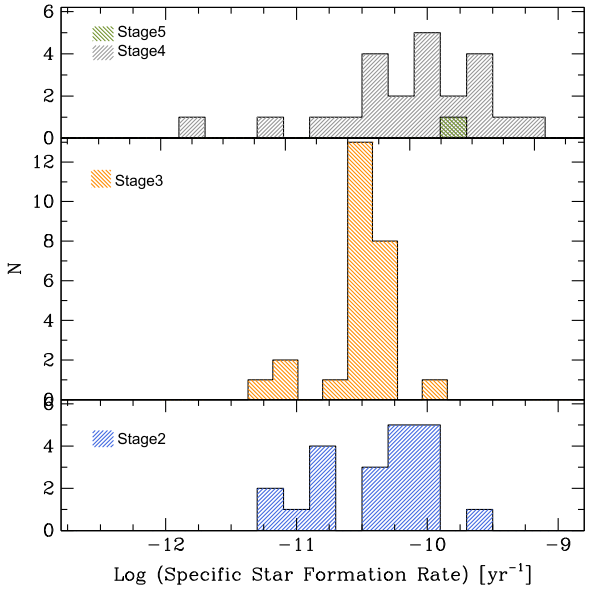

Figure 12. Left: histogram of sSFR for all 70 spiral galaxies (excluding the strong MIR AGN sources NGC 3690 and IC 694), grouped with respect to interaction strength.

Table 8
Non-parametric Tests between sSFR of Sub-samples

Sample	Null Hypothesis (KS test)	Null Hypothesis (WMW test)
Arp-Complete	0.042	0.019
Stage 2—Stage 3	0.181	0.488
Stage 3—Stage 4	0.044	0.076
Stage 2—Stage 4	0.504	0.094
Spiral Arp—Complete	0.069	0.011
Spiral Stage 2—Stage 3	0.192	0.757
Spiral Stage 3—Stage 4	0.003	0.004
Spiral Stage 2—Stage 4	0.092	0.028
All–Control	0.107	0.060
All Spirals—Control	0.0024	6×10^{-4}
Stage 2 Spirals—Control	0.152	0.041
Stage 3 Spirals—Control	0.014	0.031
Stage 4 Spirals—Control	0.001	3×10^{-4}

shows marginal significance, with a null hypothesis probability of 0.04 for the WMW test (Table 8). This is consistent with the suggestions from the overall sample that any galaxy involved in an interaction can exhibit enhanced sSFR. Lanz et al. (2013) compared sSFRs derived from SED fitting between stages for a subset of the SIGS sample. No statistical differences were found in the sSFR, but the sample sizes were small. The sSFRs presented here for the Lanz et al. (2013) do not change that result.

5.2. *Influence of sSFR with Galaxy Properties*

In addition to the time evolution of the interaction, its initial parameters such as galaxy mass, mass ratio between the systems, and galaxy separation are all thought to be important parameters for the intensity of SF triggered during an interaction (see Bournaud 2011 and references therein). Figure 13 presents the sSFR against these parameters. There is possibly a very slight decrease in sSFR at larger separations (left), although it is not statistically significant; we see no trends with any of the other parameters.

Simulations have suggested that for minor mergers the less massive system in the interaction will experience higher levels of sSFR than the more massive galaxy (Cox et al. 2008; Cox 2009). This difference in the level of triggered SFR has also been seen in observational studies (Woods & Geller 2007; Ellison et al. 2008). To investigate if this effect is seen in the SIGS spirals, we have separated the massive and less massive members of both "intermediate" (mass ratios >1:4 and <1:10) and minor mergers (mass ratio >1:10), which is presented in Figure 14. There is an indication for slightly elevated sSFR in the less massive galaxies, but this is not statistically significant.

We further probed the different interaction parameters for all spirals in the SIGS sample as a function of their interaction

Table 7
Statistical Properties of the sSFR in Different Sub-samples

Sample	N	Median ($\times10^{-11}$ yr^{-1})	Log Median (yr^{-1})	Upper Quartile (yr^{-1})	Lower Quartile (yr^{-1})	Mean ($\times10^{-11}$ yr^{-1})	Log Mean (yr^{-1})
Total	101	0.48 ± 0.08	−10.32	−10.09	−11.09	0.72 ± 0.09	−10.14
Complete	63	0.39 ± 0.08	−10.40	−10.13	−11.13	0.68 ± 0.16	−10.17
Arp	38	0.59 ± 0.17	−10.23	−9.88	−10.84	0.96 ± 0.18	−10.02
Stage 2	35	0.38 ± 0.12	−10.42	−10.09	−11.47	0.68 ± 0.16	−10.17
Stage 3	34	0.42 ± 0.06	−10.38	−10.22	−10.61	0.54 ± 0.11	−10.27
Stage 4	31	0.53 ± 0.17	−10.27	−9.89	−11.21	0.94 ± 0.19	−9.95
Stage 5	1	1.55 ± 0	−9.81	0	0	1.55 ± 0	−9.81
Spiral All	70	0.51 ± 0.06	−10.30	−10.07	−10.46	0.74 ± 0.09	−10.13
Spiral Complete	46	0.46 ± 0.07	−10.33	−10.13	−10.55	0.60 ± 0.08	−10.22
Spiral Arp	24	0.73 ± 0.14	−10.14	−9.87	−10.37	1.00 ± 0.20	−10.00
Spiral Stage 2	21	0.55 ± 0.15	−10.26	−10.10	−10.80	0.59 ± 0.11	−10.23
Spiral Stage 3	26	0.44 ± 0.04	−10.35	−10.25	−10.46	0.48 ± 0.05	−10.332
Spiral Stage 4	22	0.91 ± 0.19	−10.04	−9.84	−10.34	1.15 ± 0.23	−9.94
Spiral Stage 5	1	1.55 ± 0	−9.81	0	0	1.55 ± 0	−9.81
All Control	50	0.33 ± 0.07	−10.48	−10.28	−11.12	0.48 ± 0.09	−10.32

Note. All of these values have been derived excluding the strong MIR AGN sources NGC 3690 and IC 694.

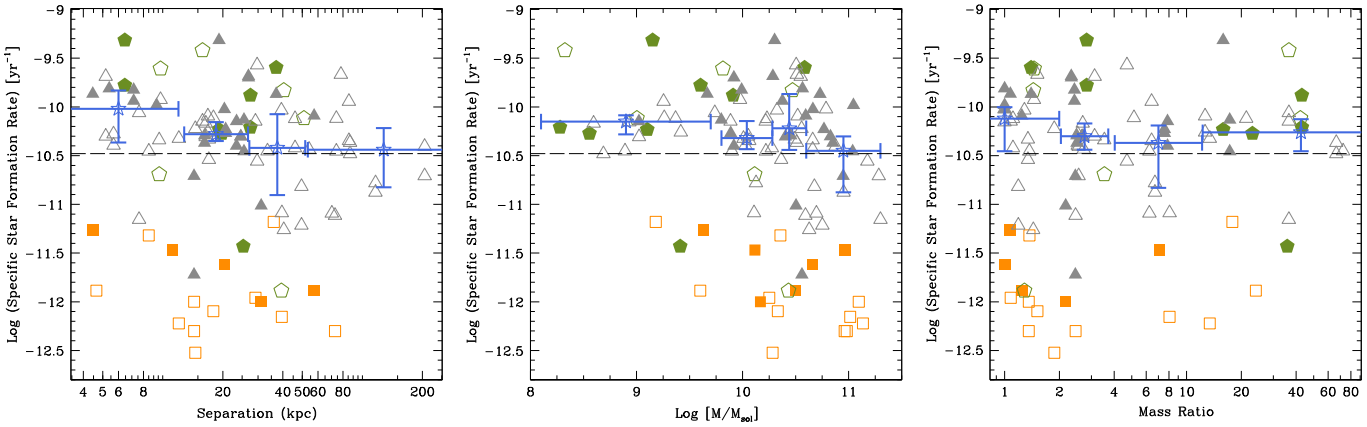

Figure 13. Left: sSFR plotted against the separation between the galaxies in each group for all 101 galaxies (excluding both saturated galaxies in Grp24, Table 1). Middle: sSFR plotted against the stellar mass of each sample galaxy. Right: sSFR against the mass ratio of the galaxies in each group. In all three panels early-type galaxies are presented as orange squares, irregular galaxies as green pentagons, and the spiral galaxies as gray triangles. Open points denote galaxies in the "Complete sample" and closed points "Arp" sample galaxies. Median values of the sSFR and upper and lower quartiles from the spiral galaxies only, calculated within each of the four bins along each of the parameters of interest, are indicated by the blue points. The horizontal dashed line indicates the median sSFR for the control sample.

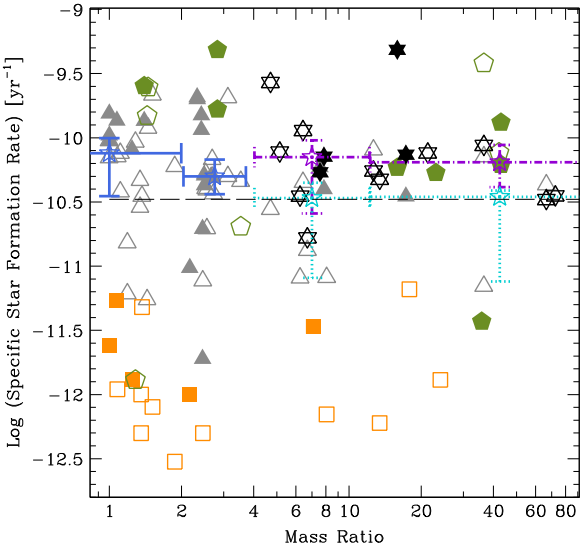

Figure 14. Scatter plot showing the sSFR against mass ratios for all spiral galaxies (as in Figure 13). Here the lower mass members of interactions with mass ratios >1:4 are indicated by the black stars. Median values of the sSFR for the intermediate and minor merger systems has been calculated from only these less massive "minor" members and are shown by the dotted–dashed purple lines, and the "massive" members by the light blue dotted lines. The median values derived from all spiral galaxies are presented by the blue solid lines. The horizontal dashed line indicates the median sSFR for the control sample.

strength. In Figure 15 the sSFR for different stage systems are plotted against separation, mass and mass ratio for all spirals. While there is no correlation of sSFR with galaxy separation, there are no Stage 2 galaxies closer than 15 kpc and only 6 with a separation less than 40 kpc. The Stage 3 galaxies seem to have a wide range of separations, and the Stage 4 systems (as well as the Stage 5 galaxy) are within 40 kpc. No correlations are found as a function of interaction strength for either mass or mass ratio, although this could be a volume effect. However, from the middle panel it can be seen that there is an absence of low-mass ($< \sim \times 10^{10}$ $M_{\odot}$) spiral galaxies with low sSFRs ($< \sim -10.50$). This dearth of low-mass quiescent systems from our sample can be explained by the rarity of these types of galaxies in the universe (cf. Bonfini 2013), which, given our sample size, are not well sampled in SIGS.

6. DISCUSSION

6.1. Early-stage SF Triggering

The interacting *spiral* galaxy sample exhibits higher sSFR than the non-interacting field spirals in our control sample (median log sSFR of −10.30 and −10.56, respectively), with both KS and WMW tests indicating that they do not arise from the same population. This result is consistent with previous studies, which have shown an increase in SFR with interactions. However, many of these papers have predominantly focused on samples selected on morphological disturbances (e.g., Smith et al. 2007; Huang & Hwang 2011), therefore biasing the surveys to stronger or move evolved interactions. In this work we have complemented these morphological samples, which would largely be classified at Stage 4 interactions in our study, with weakly interacting Stage 2 and 3 systems. A summary of the sub-classifications of interaction stage, sample classification and morphological type is presented in Table 9.

Two recent studies based on samples of galaxy pairs (with strong emission lines, indicating these galaxies are star-forming Scudder et al. 2012; Patton et al. 2013) show that these systems exhibit enhanced SFR compared to isolated star-forming galaxies (out to 150 h_{70}^{-1} kpc, or at all separations in the case of Scudder et al. 2012), with strong enhancement for separations <30 h_{70}^{-1} kpc, in line with previous work. Comparing these results to simulations (Torrey et al. 2012), Scudder et al. (2012) and Patton et al. (2013) have suggested that the increased SFR at larger separations is caused by an initial triggering of SF some time after the first perigalactic passage. In the models, SFR then decreases as the two galaxies move to wider separations with a final triggering of more violent SF at the time of coalescence (or closest approach). The plateau of SFR observed by Scudder et al. (2012) out to 80 h_{70}^{-1} kpc was shown to be a consequence of projection effects blurring the post-perigalactic increase in SFR to wider separations (where the simulations only included systems with apocenters of <70 h_{70}^{-1} kpc). Patton et al. (2013) increased the suite of simulations to include pair mergers on different eccentricities as well as impact parameters (the simulations presented in Scudder et al. (2012) only investigated the orientation of the pairs). From these extended simulations, enhanced SFR was observed out to ∼150 h_{70}^{-1} kpc with higher

values observed between ~20–100 h_{70}^{-1} kpc and strong increases in SFR with separations <10 h_{70}^{-1} kpc, in line with the observations they present.

In the sample presented here, which contains galaxies with very low SFRs which would have not been included in the Scudder et al. (2012) sample, not only do the spirals have enhanced sSFR above the field sample, but the Arp sample has a significantly higher sSFR than the Complete sample (−10.14 and −10.33, respectively). Further, even the less evolved (or overall weaker) interactions (i.e., Stage 2 galaxies) have enhanced sSFR above isolated field systems, with the more evolved Stage 4 systems showing even stronger sSFR enhancement. These results are consistent with Scudder et al. (2012) and Patton et al. (2013), where sSFR enhancement occurs over much longer timescales than previously thought. Scudder et al. (2012) further divided their pairs sample into disturbed and non-disturbed classes and compared both of these groups as a function of separation. In terms of SFR enhancement, they did not observe a difference between these two groups (although the disturbed systems do exhibit lower metallicity, which they suggest is a consequence of dilution). The similar SFR between the two groups may result from the tidal features they use to classify the systems being visible for a shorter period of time (as little as 100 Myr, Lotz et al. 2008) than the SFR enhancement (~300 Myr peak after first perigalactic passage, Scudder et al. 2012), and therefore some of the non-disturbed galaxies will have undergone their first perigalactic passage. Further, faint tidal features may not be visible in the SDSS images at the distances of the objects in their sample, and therefore some of the non-disturbed systems may actually still exhibit signs of disturbance, which would be identified with deeper, more sensitive images. The SIGS Stage 2 systems, i.e., those galaxies with no visible traces of an interaction, still exhibit an enhancement of sSFR above isolated galaxies, albeit with lower significance than for the Stage 3 and 4 galaxies. Indeed, their level of sSFR is consistent with the Stage 3 (i.e., galaxies that show weak disturbances) sample, all of which do exhibit tidal features. We therefore suggest that *some* of our Stage 2 galaxies are post-perigalactic, and as such our Stage 2 and 3 systems can be considered as part of one evolutionary stage in the interaction (i.e., between their first passage and final coalescence). However, some of the Stage 2 galaxies will be at a point before their closest approach, a time at which little to no SF is triggered. It is therefore puzzling that both stages have similar sSFR properties. The simulations of Lotz et al. (2008) suggest that in some interactions, tidal features may begin to form before there is a significant enhancement in SFR. It is therefore possible that some of the Stage 3 galaxies, despite their visible appearance, do not yet have enhanced SF and are therefore less evolved than some of the Stage 2 systems.

Table 9
Summary of Galaxy Morphologies and Sub-samples

Stage	Spiral Total (Arp/ Complete)	Early-type Total (Arp/ Complete)	Irregular Total (Arp/ Complete)	Total Total (Arp/ Complete)
2	21 (1/20)	8 (1/7)	6 (3/3)	35 (5/30)
3	26 (8/18)	4 (1/3)	4 (2/2)	34 (11/23)
4	24 (14/10)	5 (4/1)	4 (3/1)	33 (21/12)
5	1 (1/0)	…	…	1 (1/0)
Total	72 (24/48)	17 (6/11)	14 (8/6)	103 (38/65)

Note. The strong MIR AGN sources NGC 3690 and IC 694 are both included within this summary table. Both are within the Complete sample and have been classified as Stage 4 galaxies.

6.2. Dependence of sSFR With Separation

Scudder et al. (2012) and Patton et al. (2013) used galaxy separation as the main parameter to compare to the sSFR. Both studies determined that galaxies within ~20–30 h_{70}^{-1} kpc have significantly enhanced sSFR compared to the wider systems. The authors suggest this sSFR is predominantly driven by galaxies just at the point of coalescence. In fact, Scudder et al. (2012) reported that strong starbursts in their sample (10 times as strong as the control) are rare and more likely to be found in the close pairs (<30 h_{70}^{-1} kpc). We do not observe this same marked increase in sSFR, which can be explained by our sample selection. This was defined to probe the initial stages of interactions, not systems just at the point of nuclear coalescence (for example the K85 Arp sample *excluded* systems where two distinct discs could not be identified). This results in only one Stage 5 system (Grp3) at an advanced merger stage and consequently does not include the very strong starbursts seen by Scudder et al. (2012). By including early-stage systems, we have determined that there is enhanced sSFR at all separations, which is consistent with previous results. However, SIGS

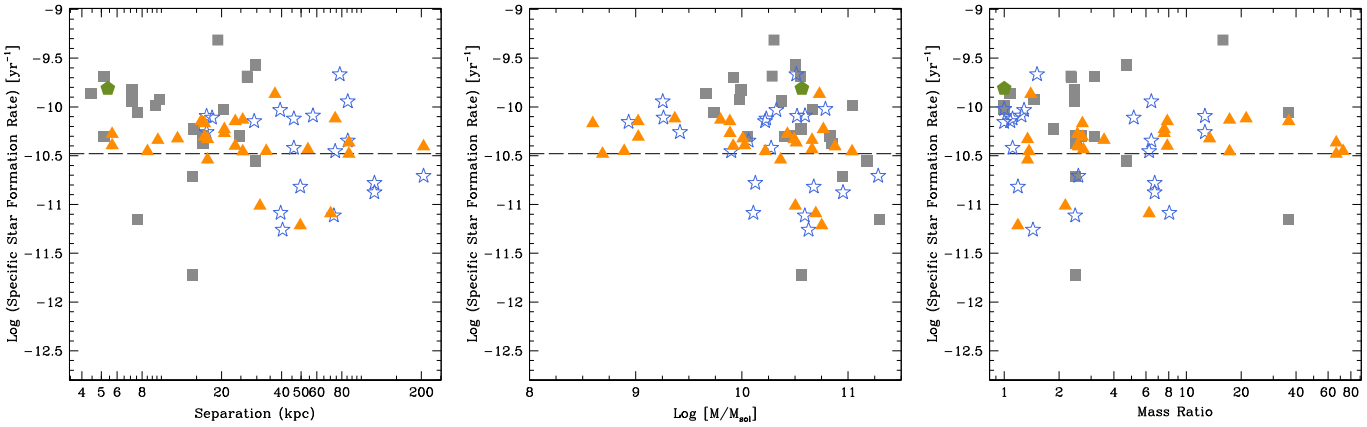

Figure 15. Left: sSFR plotted against separation (Table 1) for all spiral galaxies. Middle: mass against sSFR. Right: mass ratio against sSFR. In all three panels Stage 2 galaxies are indicated by blue stars, Stage 3 systems by orange triangles and Stage 4 systems by gray squares. The Stage 5 system is indicated by the green pentagon. The horizontal dashed line indicates the median sSFR for the control sample.

contains only two pair systems with separations >100 kpc; Grp43 and Grp46, therefore we have insufficient statistics to determine if sSFR declines or is constant at greater separations than this. Further, Figure 15 shows that the majority of our Stage 2 galaxies have separations of $\geqslant$40 kpc while still exhibiting enhanced sSFR. This behavior is consistent with the interpretation presented by Scudder et al. (2012), who suggested that some systems with large separations (up to 80 h_{70}^{-1} kpc in their work) are post-perigalactic systems which have had sufficient time for their tidal features to disappear. This result indicates that studies selecting interactions based on disturbed morphology *are* missing an important component of the overall SFR resulting from galaxy interactions.

7. CONCLUSIONS

The MIR *Spitzer* observations of interacting galaxies drawn from the K85 sample has provided us with the opportunity to study a wide range of galaxy interactions, including systems exhibiting no morphological disturbances. Our sample contains 103 galaxies (in 48 interacting systems) with a wide range of morphologies (72 spirals, 12 irregulars, and 19 elliptical galaxies), mass ($2 \times 10^8 - 2 \times 10^{11}$ $M_\odot$), and mass ratios (1:1–1:73). Through *Spitzer* IRAC and MIPS 24 μm observations of all 103 galaxies, we have been able to determine the sSFR of each system and investigate correlations between this value and galaxy properties. The purpose of this work is to understand the process of triggering SF during the interaction process and therefore we have focused on correlations involving the (non-AGN) spiral galaxies.

Our main results can be summarized as follows.

1. Statistically the *spiral* galaxies sample (70 galaxies, excluding the two systems we have identified as AGN) exhibit enhanced sSFR above our control field sample with median log sSFR of −10.30 and −10.48, respectively.
2. We observe very little variation of the enhanced sSFR with separation. The lack of significantly enhanced sSFR in close pairs, which has been identified in previous galaxy pair surveys, can be attributed to our selection criteria, where strongly interacting galaxies without two discernible disks have been excluded. These late stage mergers are predominantly the systems that exhibit greatly enhanced sSFR. Determining the elevated sSFR to separations ∼100 kpc corroborates the work of Scudder et al. (2012) and Patton et al. (2013), both of whom observe this same plateau in pair samples to 80 h_{70}^{-1} kpc and 150 h_{70}^{-1} kpc, respectively. The galaxies with enhanced sSFR at large separations are likely post-perigalactic systems.
3. Mass and mass ratios are not associated with variations of sSFR, although there is a slight suggestion that the less massive galaxies in the "intermediate" (1:4–1:10) and minor (>1:10) mergers have higher sSFRs than those of the massive members.
4. Galaxies exhibiting morphological disturbances (the "Arp" sample) have sSFR greater than those without (the "Complete" sample; median log sSFR −10.14 and −10.33, respectively). This confirms the more evolved (or stronger interaction) state of these systems.
5. The Stage 2 (no optical signs of interaction) and Stage 3 galaxies (moderate tidal features) have similar sSFRs (both of which are above the control sSFR value). The Stage 4 galaxy sample (strong interaction features) on the other hand has a statistically higher median values than stages 2 and 3 (−10.04 versus −10.26 and −10.35, respectively).
6. Most of the Stage 4 galaxies have projected separations within 40 kpc whereas Stage 3 systems are found across all separations. The Stage 2 galaxies on the other hand are predominantly at larger separations (>40 kpc). We suggest that *some* of these systems are likely to be the post-perigalactic galaxies proposed by Scudder et al. (2012) and Patton et al. (2013), where the evolution of the system from the time of the first passage has led to the fading of the morphological interaction signatures to undetectable levels. The existence of these galaxies indicates that the induced disturbance in the ISM and the ongoing process of large-scale gas flows and consequently enhanced SFR is a long-lived event. However, without the ability to determine which of our Stage 2 galaxies are pre and post-perigalactic systems, we cannot identify the point at which this process was initially triggered. Enhanced sSFR even without tidal features highlights the importance of using a sample of wide separation galaxy pairs when studying SFR in interactions instead of samples based on disturbed morphology.

We would like to thank the referee for useful comments which have improved our paper. This work makes use of observations made with the *Spitzer Space Telescope*, which is operated by the Jet Propulsion Laboratory, California Institute of Technology, under a contract with NASA. This work is based in part on the IRAC post-BCD processing software "IRACproc" developed by Mike Schuster, Massimo Marengo, and Brian Patten at the Smithsonian Astrophysical Observatory. We acknowledge support in part from NASA grant NNX10AD68G, NASA JPL RSA 1369566, and NASA JPL RSA 717352. N.J.B. would like to thank the physics department at the University of Crete and IESL Foundation for Research and Technology for their hospitality during part of this work.

REFERENCES

Alonso-Herrero, A., Rieke, G. H., Rieke, M. J., et al. 2006, ApJ, 650, 835
Alonso-Herrero, A., Rieke, G. H., Colina, L., et al. 2009, ApJ, 697, 660
Alonso-Herrero, A., Roche, P. F., Esquej, P., et al. 2013, arXiv:1311.3446
Arp, H. 1966, ApJS, 14, 1
Ashby, M. L. N., Mahajan, S., Smith, H. A., et al. 2011, PASP, 123, 1011
Bendo, G. J., Calzetti, D., Engelbracht, C. W., et al. 2007, MNRAS, 380, 1313
Bertin, E., & Arnouts, S. 1996, A&AS, 117, 393
Bonfini, P. 2013, PhD thesis, Univ. of Crete
Bournaud, F. 2011, in EAS Publications Ser. 51, ed. C. Charbonnel, & T. Montmerle (Cedex: EDP Sciences), 107
Bournaud, F., Combes, F., & Jog, C. J. 2004, A&A, 418, L27
Bushouse, H. A. 1987, ApJ, 320, 49
Calzetti, D., Kennicutt, R. C., Jr., Bianchi, L., et al. 2005, ApJ, 633, 871
Calzetti, D., Kennicutt, R. C., Engelbracht, C. W., et al. 2007, ApJ, 666, 870
Calzetti, D., Wu, S.-Y., Hong, S., et al. 2010, ApJ, 714, 1256
Cox, T. J. 2009, in ASP Conf. Ser. 419, Galaxy Evolution: Emerging Insights and Future Challenges, ed. S. Jogee et al. (San Francisco, CA: ASP), 235
Cox, T. J., Jonsson, P., Primack, J. R., & Somerville, R. S. 2006, MNRAS, 373, 1013
Cox, T. J., Jonsson, P., Somerville, R. S., Primack, J. R., & Dekel, A. 2008, MNRAS, 384, 386
Dahari, O. 1985, ApJS, 57, 643
Dale, D. A., Bendo, G. J., Engelbracht, C. W., et al. 2005, ApJ, 633, 857
Dale, D. A., Cohen, S. A., Johnson, L. C., et al. 2009, ApJ, 703, 517

de Vaucouleurs, G., de Vaucouleurs, A., Corwin, H. G., et al. 1991, Third Reference Catalogue of Bright Galaxies, Vol. 1–3, XII, (Berlin: Springer)
di Matteo, T., Springel, V., & Hernquist, L. 2005, Natur, 433, 604
Dopita, M. A., Pereira, M., Kewley, L. J., & Capaccioli, M. 2002, ApJS, 143, 47
Ellison, S. L., Patton, D. R., Simard, L., & McConnachie, A. W. 2008, AJ, 135, 1877
Fazio, G. G., Hora, J. L., Allen, L. E., et al. 2004, ApJS, 154, 10
Freedman Woods, D., Geller, M. J., Kurtz, M. J., et al. 2010, AJ, 139, 1857
Gallagher, S. C., Johnson, K. E., Hornschemeier, A. E., Charlton, J. C., & Hibbard, J. E. 2008, ApJ, 673, 730
Graham, A. W., & Driver, S. P. 2005, PASA, 22, 118
Ho, L. C., Filippenko, A. V., & Sargent, W. L. W. 1997, ApJS, 112, 315
Hopkins, P. F., Hernquist, L., Cox, T. J., & Kereš, D. 2008, ApJS, 175, 356
Huang, M.-L., & Hwang, C.-Y. 2011, ApJ, 734, 99
Hunter, D. A., & Elmegreen, B. G. 2004, AJ, 128, 2170
Johnson, K. E., Hibbard, J. E., Gallagher, S. C., et al. 2007, AJ, 134, 1522
Kampczyk, P., Lilly, S. J., de Ravel, L., et al. 2013, ApJ, 762, 43
Keel, W. C., Kennicutt, R. C., Jr., Hummel, E., & van der Hulst, J. M. 1985, AJ, 90, 708
Kennicutt, R. C., Jr., Roettiger, K. A., Keel, W. C., van der Hulst, J. M., & Hummel, E. 1987, AJ, 93, 1011
Kennicutt, R. C., Jr., Armus, L., Bendo, G., et al. 2003, PASP, 115, 928
Kennicutt, R. C., Jr., Hao, C.-N., Calzetti, D., et al. 2009, ApJ, 703, 1672
Kewley, L. J., Heisler, C. A., Dopita, M. A., & Lumsden, S. 2001, ApJS, 132, 37
Kron, R. G. 1980, ApJS, 43, 305
Lanz, L., Zezas, A., Brassington, N., et al. 2013, ApJ, 768, 90
Lanz, L., Zezas, A., Brassington, N., et al. 2014, ApJ, 785, 39
Larson, R., & Tinsley, B. 1978, ApJ, 219, 46
Li, Y., Crocker, A. F., Calzetti, D., et al. 2013, ApJ, 768, 180
Lonsdale, C. J., Smith, H. E., Rowan-Robinson, M., et al. 2003, PASP, 115, 897
Lotz, J. M., Jonsson, P., Cox, T. J., & Primack, J. R. 2008, MNRAS, 391, 1137
Lutz, D. 1992, A&A, 259, 462
Mann, H., & Whitney, D. 1947, Ann. Math. Statist, 18, 50
Mihos, J. C., & Hernquist, L. 1996, ApJ, 464, 641
Mould, J. R., Huchra, J. P., Freedman, W. L., et al. 2000, ApJ, 529, 786
Mullaney, J. R., Alexander, D. M., Goulding, A. D., & Hickox, R. C. 2011, MNRAS, 414, 1082
Murphy, E. J., Condon, J. J., Schinnerer, E., et al. 2011, ApJ, 737, 67
Patton, D. R., Torrey, P., Ellison, S. L., Mendel, J. T., & Scudder, J. M. 2013, MNRAS, 433, L59
Pérez-Torres, M. A., Alberdi, A., Romero-Cañizales, C., & Bondi, M. 2010, A&A, 519, L5
Rieke, G. H., Alonso-Herrero, A., Weiner, B. J., et al. 2009, ApJ, 692, 556
Rieke, G. H., Young, E. T., Engelbracht, C. W., et al. 2004, ApJS, 154, 25
Sanders, D. B., Soifer, B. T., Elias, J. H., et al. 1988, ApJ, 325, 74
Saunders, W., Sutherland, W. J., Maddox, S. J., et al. 2000, MNRAS, 317, 55
Schuster, M. T., Marengo, M., & Patten, B. M. 2006, in SPIE Conf. Ser. 6270
Scudder, J. M., Ellison, S. L., Torrey, P., Patton, D. R., & Mendel, J. T. 2012, MNRAS, 426, 549
Smith, B. J., Struck, C., Hancock, M., et al. 2007, AJ, 133, 791
Stern, D., Eisenhardt, P., Gorjian, V., et al. 2005, ApJ, 631, 163
Struck, C. 1999, PhR, 321, 1
Torrey, P., Cox, T. J., Kewley, L., & Hernquist, L. 2012, ApJ, 746, 108
Tully, R. B., Shaya, E. J., Karachentsev, I. D., et al. 2008, ApJ, 676, 184
Woods, D. F., & Geller, M. J. 2007, AJ, 134, 527
Wu, H., Cao, C., Hao, C.-N., et al. 2005, ApJL, 632, L79
Xu, C. K., Domingue, D., Cheng, Y.-W., et al. 2010, ApJ, 713, 330
Young, L. M., Bendo, G. J., & Lucero, D. M. 2009, AJ, 137, 3053
Zhu, Y.-N., Wu, H., Cao, C., & Li, H.-N. 2008, ApJ, 686, 155
Zhu, Y.-N., Wu, H., Li, H.-N., & Cao, C. 2010, RAA, 10, 329